Adaptation of pancreatic cancer cells to nutrient deprivation is reversible and requires glutamine synthetase stabilization by mTORC1

Pei-Yun Tsai[a,b,1], Min-Sik Lee[a,b,c,1], Unmesh Jadhav[d,e,f,g], Insia Naqvi[a], Shariq Madha[d,e], Ashley Adler[a,c], Meeta Mistry[h], Sergey Naumenko[h], Caroline A. Lewis[i], Daniel S. Hitchcock[c], Frederick R. Roberts[j], Peter DelNero[a,k], Thomas Hank[l], Kim C. Honselmann[l], Vicente Morales Oyarvide[d], Mari Mino-Kenudson[m], Clary B. Clish[c], Ramesh A. Shivdasani[d,e,f,g,n], and Nada Y. Kalaany[a,b,c,2]

[a]Division of Endocrinology, Boston Children's Hospital, Boston, MA, USA.
[b]Department of Pediatrics, Harvard Medical School, Boston, MA, USA.
[c]Broad Institute of MIT and Harvard, Cambridge, MA, USA.
[d]Department of Medical Oncology, Dana-Farber Cancer Institute, Boston, MA, USA.
[e]Center for Functional Cancer Epigenetics, Dana-Farber Cancer Institute, Boston, MA, USA.
[f]Department of Medicine, Brigham and Women's Hospital, Boston, MA, USA.
[g]Department of Medicine, Harvard Medical School, Boston, MA, USA.
[h]Bioinformatics Core, Harvard T.H. Chan School of Public Health, Boston, MA, USA.
[i]Whitehead Institute for Biomedical Research, Cambridge, MA, USA.
[j]FUJIFILM VisualSonics Inc., Toronto, ON, Canada.
[k]Cancer Prevention Fellowship Program, Division of Cancer Prevention, National Cancer Institute, Bethesda, MD, USA.
[l]Department of Surgery, Massachusetts General Hospital and Harvard Medical School, Boston, MA, USA.
[m]Department of Pathology, Massachusetts General Hospital and Harvard Medical School, Boston, MA, USA.
[n]Harvard Stem Cell Institute, Cambridge, MA, USA.
[1]P.T. and M.-S.L. contributed equally to this work.
[2]To whom correspondence should be addressed. Email: nada.kalaany@childrens.harvard.edu

Abstract

Pancreatic ductal adenocarcinoma (PDA) is a lethal, therapy-resistant cancer that thrives in a highly desmoplastic, nutrient-deprived microenvironment. Several studies investigated the effects of depriving PDA of either glucose or glutamine alone. However, the consequences on PDA growth and metabolism of limiting both preferred nutrients have remained largely unknown. Here, we report the selection for clonal human PDA cells that survive and adapt to limiting levels of both glucose and glutamine. We find that adapted clones exhibit increased growth *in vitro* and enhanced tumor-forming capacity *in vivo*. Mechanistically, adapted clones share common transcriptional and metabolic programs, including amino acid use for *de novo* glutamine and nucleotide synthesis. They also display enhanced mTORC1 activity that prevents the proteasomal degradation of glutamine synthetase (GS), the rate-limiting enzyme for glutamine synthesis. This phenotype is notably reversible, with PDA cells acquiring alterations in open chromatin upon adaptation. Silencing of GS suppresses the enhanced growth of adapted cells and mitigates tumor growth. These findings identify non-genetic adaptations to nutrient deprivation in PDA and highlight GS as a dependency that could be targeted therapeutically in pancreatic cancer patients.

Significance

Pancreatic ductal adenocarcinoma (PDA) is a highly lethal malignancy with no effective therapies. PDA aggressiveness partly stems from its ability to grow within a uniquely dense stroma restricting nutrient access. This study demonstrates that PDA clones that survive chronic nutrient deprivation acquire reversible non-genetic adaptations allowing them to switch between metabolic states optimal for growth under nutrient-replete or nutrient-deprived conditions. One contributing factor to this adaptation mTORC1 activation, which stabilizes glutamine synthetase

53 (GS) necessary for glutamine generation in nutrient-deprived cancer cells. Our findings imply
54 that although total GS levels may not be a prognostic marker for aggressive disease, GS
55 inhibition is of high therapeutic value, as it targets specific cell clusters adapted to nutrient
56 starvation, thus mitigating tumor growth.
57
58 **Introduction**
59 With a steady rise in incidence and a poor 5-year survival rate of ~ 9%, PDA is now the third leading
60 cause of cancer death in the US (1, 2). Oncogenic *KRAS* mutations are highly prevalent in PDA (>
61 90%), driving many of its distinctive metabolic features (3, 4). These include the macropinocytic uptake
62 of extracellular macromolecules, the recycling of intracellular components (5-8), and the re-direction of
63 glycolytic and glutaminolytic intermediates into anabolic and redox-controlling pathways required for
64 PDA growth (9, 10). However, whether these alterations are sufficient to account for the ability of PDA
65 to thrive in a seemingly hostile *in vivo* microenvironment, where abnormal vasculature and exuberant
66 stroma restrict nutrient access, remains unknown.
67 Because nutrient availability largely dictates metabolic behavior (11), the relevance of studying
68 tumor metabolism within the native environment has been recently underscored (12-16). Although
69 culture media composition can be modulated to mimic circulating metabolite levels (17, 18), this
70 modulation may not accurately reflect the tumor metabolic microenvironment. In particular, levels of
71 glucose and glutamine, two of the most abundant and tumor-preferred nutrients in the circulation, can be
72 limiting in PDA tumors, compared to benign adjacent tissue (7), and significantly lower within tumor
73 cores, compared to the periphery (19, 20). Paradoxically, both glucose and glutamine are routinely
74 supplemented in culture media at levels that are significantly higher than the circulation: 11mM glucose
75 and 2mM glutamine in RPMI compared to ~ 5.5mM glucose and 0.6mM glutamine in serum (21).

76 Although prior studies focused on depriving tumor cells of either glucose or glutamine alone (10, 22-
77 25), how PDA cells survive and proliferate under limiting levels of both major nutrients is not well
78 understood.

79 To investigate this, we selected for clonal PDA cells that survive and adapt to limiting levels of
80 both glucose and glutamine. We find that the adapted clones have enhanced proliferation *in vitro* and
81 tumor-forming capacity *in vivo*. They also share common signaling, transcriptional and metabolic
82 alterations that are acquired upon adaptation. These include a post-translational role for mTORC1
83 signaling in the stabilization of glutamine synthetase (GS), and the use of amino acids for the synthesis
84 of glutamine and nucleotides. Of note, this phenotype is reversible, implicating epigenetic alterations in
85 the adaptation process, and highlighting GS as a candidate for therapeutic targeting in pancreatic cancer.
86

87 **Results**

88 **PDA cells adapted to low glucose / low glutamine have enhanced growth *in vitro* and *in vivo***

89 To test whether pancreatic cancer cells can survive and adapt to harsh nutrient-deprived conditions, we
90 cultured seven human PDA cell lines (AsPC-1, BxPC-3, HPAC, MIA PaCa-2, PANC-1, SUIT-2 and
91 PA-TU-8988T, herein termed 8988T) in customized low glucose (0.5mM) and low glutamine (0.1mM),
92 medium (L-L). These modifications represent ~20-fold reduction from standard RPMI medium, herein
93 referred to as high glucose-high glutamine (H-H) and 5- to 10-fold decrease from human serum levels
94 (21) (Fig. 1*A*); both L-L and H-H media were supplemented with 10% dialyzed fetal bovine serum
95 (FBS). Consistent with the requirement of glucose and glutamine for PDA growth (9, 10), most PDA
96 cells died within two weeks of culture in L-L medium, despite media replenishment every 2-3 days (Fig.
97 1*B* and Fig. S1*A*). However, rare surviving cells were able to slowly proliferate past the second week,
98 particularly in SUIT-2 and 8988T, followed by MIA-PaCa-2 (Fig. 1*B* and and Fig. S1*B*). Distinct

99 genetic lesions frequently found in PDAC did not explain the differential adaptive capacity of these cell
100 lines to nutrient deprivation (Fig. S1*C*). The surviving cells in SUIT-2 and 8988T gradually gave rise to
101 adapted clones, 3 of which (A-C4, C-5 and C-6) were selected for further analysis (Fig. 1*A*). Adapted
102 clones were then studied in comparison to non-adapted clones (NA-C1, C-2 and C-3), which were
103 isolated from the corresponding parental PDA lines grown under H-H conditions (Fig.1*A*). All clones
104 were subsequently passaged every 3-4 days for use in experiments.

105 To assess their *in vitro* growth potential, adapted and non-adapted cells were first subjected to a
106 7-day proliferation assay performed without media replenishment. Whereas no significant differences
107 were detected in H-H medium conditions (Fig. S2*A* and *B*), adapted cells from both lines showed
108 enhanced proliferative capacity (Fig. 1*C*) and decreased cell death (Fig. 1*D*), compared to non-adapted
109 clones, in L-L medium. In a colony formation assay, adapted clones tended to generate a larger number
110 of colonies in L-L but not in H-H medium (Fig. 1*E* and Fig. S2*C*). When plated under 3-dimensional (3-
111 D) culture conditions, adapted 8988T cells formed a significantly higher number of spheres (Fig. S2*D*)
112 with a larger area (Fig. 1*F*) than non-adapted clones in L-L, but not H-H medium (Fig. S2*E* and *F*).
113 SUIT-2 clones formed a similar number of spheres, independent of the medium or adaptation (Fig. S2*D*
114 and *E*). However, SUIT-2 spheres tended to be larger in adapted, compared to non-adapted clones, when
115 cultured under L-L, but not H-H conditions (Fig. 1*F* and Fig. S2*F*).

116 Because autophagy and macropinocytosis are well-recognized dependencies in PDA (3, 5, 6, 8),
117 we assessed their potential contribution to the enhanced proliferation of the adapted clones under
118 nutrient-limiting conditions. No differential increase in autophagic flux was observed in adapted cells,
119 compared to non-adapted controls in L-L medium (Fig. S3*A*). Moreover, uptake of
120 tetramethylrhodamine (TMR)-labeled dextran, an indicator of macropinocytosis, was not further
121 increased in the adapted, compared to non-adapted cells, under L-L conditions (Fig. S3*B*). These data

122 indicate that surviving PDA cells that adapt to chronic glucose and glutamine deprivation acquire a
123 proliferative potential that depends on processes other than autophagy or macropinocytosis.
124 To test whether the adaptation-mediated *in vitro* phenotype could be translated *in vivo*, adapted
125 and non-adapted SUIT-2 PDA clonal cells were orthotopically injected into the pancreas of B6.Rag1$^{-/-}$
126 mice (Fig. 1*G* and *H* and Fig. S2*G*). Within the span of 6 weeks, only 8 out of 13 non-adapted cell
127 injections derived from 2 different clones formed detectable, yet smaller tumors (~ 119 mm^3 in volume;
128 197 mg in weight) with delayed latency (Fig. 1*G* and *H*). In contrast, 14 of 14 adapted clonal cell
129 injections produced tumors that were detected as early as week 3 by ultrasound (Fig. 1*G*). On week 6,
130 these tumors were approximately 4-fold larger in volume (~ 463 mm^3) and over 2-fold heavier (~ 436
131 mg) than tumors from non-adapted clones (Fig. 1*G* and *H* and Fig. S1*G*). Moreover, two mice bearing
132 the largest tumors from adapted cells (Fig. 1*G*, clone 5, red arrow) succumbed to tumor burden on week
133 5 and were therefore not included in the analyses at week 6 (Fig. 1*G* and *H*). These results demonstrate
134 that metabolic adaptation to a nutrient-deprived environment can endow cancer cells with higher growth
135 fitness, allowing tumors to survive and thrive during periods of nutrient starvation both *in vitro* and *in*
136 *vivo*.
137
138 **Adapted PDA clones display altered amino acid and nucleotide metabolism coupled with**
139 **enhanced mTORC1 signaling**
140 To identify transcriptional alterations that convey enhanced proliferative potential to PDA upon
141 adaptation to nutrient deprivation, we used RNA-Seq to profile transcripts in SUIT-2 clones under L-L
142 conditions. Gene set enrichment analysis (GSEA) revealed significant positive enrichment in the
143 adapted clones for pathways involved in purine and pyrimidine metabolism (Fig. S4*A* and *B*) and amino
144 acid metabolism (Fig. S4*C*-*F*), and negative enrichment for genes that suppress or are negatively

145 correlated with the mammalian target of rapamycin complex 1 (mTORC1) signaling pathway (Fig.
146 S4*G*). Metabolic profiling of SUIT-2 clones treated for 24 hours with H-H or L-L medium yielded an
147 adaptation signature that largely overlaps with the altered transcriptomes (Fig. S5*A* and *B*). Compared to
148 H-H, all clones under L-L conditions displayed markedly higher levels of intracellular amino acids (Fig.
149 S5*A*), except for alanine, glutamine, glutamate and aspartate, consistent with glutamine deprivation and
150 indicative of enhanced autophagy. This increase in amino acids was significantly suppressed in the
151 adapted clones, compared to non-adapted controls, suggesting enhanced utilization of intracellular
152 amino acids (Fig. 3*E*, relative levels between 2 groups in L-L and Fig. S5*A*, relative levels among all 4
153 groups in L-L and H-H). Furthermore, non-adapted cells showed significant accumulation of mono- and
154 di-nucleotides and their biosynthetic precursors, reflecting decreased DNA synthesis. In contrast, the
155 adapted clones displayed a nucleotide biosynthesis profile that closely mirrors that of PDA clones under
156 H-H conditions, consistent with enhanced proliferation. This profile included lower levels of mono- and
157 di-nucleotide phosphates, used to generate tri-nucleotide phosphates, which differentially accumulate in
158 the adapted clones (Fig. 2*A*, relative levels between 2 groups in L-L and Fig. S5*A*, relative levels among
159 4 groups in L-L and H-H). Indeed, although *de novo* pyrimidine synthesis was higher under H-H
160 compared to L-L conditions, a differential increase upon adaptation was observed only under L-L
161 conditions (Fig. 2*B*). This was evident in doubling of ^{14}C incorporation into DNA, 40 hours after
162 labeling of cells with ^{14}C-aspartate (Fig. 2*B*).

163 Signaling downstream of mTORC1 can induce *de novo* pyrimidine synthesis through activation
164 of the rate-limiting enzyme "CAD" or carbamoyl-phosphate synthetase 2, aspartate transcarbamoylase,
165 dihydroorotase (26). Since GSEA also indicated a potential increase in mTORC1 activity in adapted
166 clones under L-L conditions (Fig. S4*G*), we investigated a role for mTORC1 in the adaptation of the
167 PDA clones to nutrient deprivation. Compared to non-adapted clones, adapted SUIT-2 and 8988T cells

168 showed increased phosphorylation levels of CAD on Serine 1859, a site of ribosomal S6-Kinase (S6K1)
169 activity (Fig. 2*C*). This increase was particularly striking under L-L conditions. Importantly, it was
170 mirrored by enhanced mTORC1 activity, as evidenced by sustained phosphorylation of its downstream
171 effectors S6K1 and 4E-binding protein (4E-BP1), despite nutrient deprivation (Fig. 2*C*). Consistently,
172 the adapted clones displayed enhanced sensitivity to higher levels of the mTORC1 inhibitor rapamycin
173 (1 μM-20μM), as demonstrated by decreased live cell number over a 48-hour treatment (Fig. S6*B*). On
174 the other hand, no significant changes were detected in the phosphorylation levels of ERK1/2
175 downstream of activated KRAS. Moreover, levels of AKT phosphorylation (T308) were decreased in
176 adapted clones (Fig. S6*A*), consistent with mTORC1-AKT negative feedback loops (27-29).
177
178 **Adapted PDA clones have enhanced glutamine synthesis**
179 Glutamine is a pleiotropic amino acid required for protein synthesis and numerous anabolic reactions in
180 proliferating cells (22). We therefore asked whether the adapted clones have induced *de novo* glutamine
181 synthesis under L-L conditions. mRNA levels of glutamine synthetase (GS, also termed GLUL), which
182 catalyzes the condensation of glutamate and ammonium to generate glutamine (Fig. 3*A*), were only
183 moderately increased in adapted clones (Fig. S7*A*). However, GS protein levels were markedly induced
184 in adapted clones from both PDA cell lines, compared to non-adapted controls (Fig. 3*B*). This occurred
185 only under L-L conditions, as no clones harbored detectable levels of GS in H-H medium, independent
186 of adaptation (Fig. 3*B*). Although these findings are consistent with a glutamine-dependent post-
187 translational regulation of GS (30, 31), it is noteworthy that non-adapted clones only displayed a mild to
188 no increase in GS levels 24 hours following exposure to L-L medium (Fig. 3*B*), implying differential
189 metabolic rewiring in the PDA clones upon adaptation to prolonged glutamine deprivation. Importantly,
190 GS protein levels were mirrored by its enzymatic activity levels, as demonstrated by metabolic tracing

191 of ^{15}N-ammonium chloride (NH_4Cl) in SUIT-2 cells (Fig. 3*C*). Because glutamate dehydrogenase
192 (GDH, also termed GLUD) catalyzes the reductive amination of alpha-ketoglutarate (α-KG) to generate
193 glutamate (Fig. 3*A*), a moderate increase was observed in the ^{15}N-glutamate fraction between H-H and
194 L-L conditions in SUIT-2 cells (~18% vs 25%), independent of adaptation (Fig. 3*C*). This suggested the
195 use by the adapted cells of newly generated glutamate to synthesize glutamine. Indeed, adapted clones
196 cultured in L-L medium had a marked increase in ^{15}N-glutamine (M+1) fraction, generated from either
197 condensation of ^{15}N-ammonium and unlabeled glutamate, or unlabeled ammonium and GDH-derived
198 ^{15}N-glutamate, compared to non-adapted controls (30% vs 8%, respectively). This increase was also
199 observed in the (M+2) labeled fraction, which is generated when both substrates are labeled (8% in
200 adapted vs 2% in non-adapted cells). On the other hand, ^{15}N-glutamine levels were either undetectable
201 or minimally detected in the PDA clones under H-H conditions, independent of adaptation (Fig. 3*C*).
202 These data indicate that only PDA clones that survive and adapt to long-term glutamine deprivation are
203 able to induce GS protein levels under L-L conditions, so as to increase GS-mediated glutamine
204 synthesis.
205
206 **Adapted PDA cells use amino acids as a nitrogen source for glutamine and nucleotide synthesis**
207 In addition to reductive amination of α-KG through GDH (Fig. 3*A*), the transamination reaction
208 catalyzed by branched chain amino acid (BCAA) transaminase (BCAT1/2) could contribute to the
209 generation of mitochondrial glutamate that is then used for glutamine synthesis. Moreover, aspartate
210 transaminase (GOT1/2, also termed AST1/2) could transfer the nitrogen from glutamate to aspartate, a
211 key substrate in nucleotide biosynthesis (Fig. 3*D*). Global metabolite profiling of the PDA clones
212 revealed a significant decrease in amino acid levels, including the branched chain amino acids (BCAA)
213 leucine, valine and isoleucine in all adapted clones, suggesting enhanced amino acid utilization by the

214 more proliferative cells (Fig. 3*E* and Fig. S5*A*). Indeed, adapted clones showed increased protein levels
215 of BCAT2 and GOT2 in SUIT-2 cells, whereas BCAT1 and GOT1 were increased in 8988T cells (Fig.
216 S7*B*). ^{15}N-leucine tracing demonstrated that the labeled nitrogen incorporates at significantly higher
217 levels into glutamate, aspartate and intermediates in nucleotide synthesis in adapted, compared to non-
218 adapted clones under L-L conditions (Fig. 3*F*). Moreover, the ^{15}N-labeled fraction of glutamine was
219 minimal (1%) under nutrient-replete H-H conditions, whereas a marked 5-fold increase in ^{15}N-glutamine
220 was detected under L-L conditions, specifically in the adapted clones (Fig. 3*F*). These data imply that
221 BCAAs are a significant source for *de novo* synthesis of glutamine and nucleotides in PDA cells adapted
222 to L-L conditions.
223

224 **Deprivation of glutamine rather than glucose is a larger contributor to the enhanced proliferative**
225 **fitness of adapted PDA cells**

226 To distinguish the contributions of glucose versus glutamine to the adaptability phenotype, we
227 selected for SUIT-2 and 8988T parental cells that survive and adapt to deprivation of either glucose-only
228 (low glucose-high glutamine; L-H medium), glutamine-only (high glucose-low glutamine; H-L
229 medium), or both glucose and glutamine (L-L). We then compared their proliferative capacity to that of
230 control non-adapted parental cells that were maintained in nutrient replete (H-H) medium. Under H-H
231 medium, enhanced proliferation of adapted cells was only observed on the last day of the assay (day 7),
232 when nutrients become more depleted in the non-replenished medium (Fig. S8*A*, top panels). When
233 grown in L-L medium however, the markedly enhanced proliferative capacity of cells adapted to L-L
234 conditions could be mostly attributed to adaptation to glutamine deprivation, rather than deprivation of
235 glucose. This is evident in the growth curves of H-L adapted cells that more closely mimic those of L-L
236 adapted cells; in contrast, L-H adapted cells only displayed minimal to moderately enhanced

237 proliferative fitness (Fig. S8*A*, bottom panels). Consistently, GS protein levels were most induced in H-
238 L compared to L-H adapted clones in both cell lines (Fig. S8*B*).
239 We next assessed the effects of short-term deprivation of either glucose or glutamine, on altered
240 metabolism, mTORC1 activity and GS levels in the L-L adapted SUIT-2 clones (Fig. 1*A*). Except for
241 metabolites in glycolysis (marked with a star), deprivation of glutamine alone (H-L), rather than glucose
242 (L-H), more closely mimicked the metabolic alterations observed upon deprivation of both nutrients (L-
243 L). These include changes in levels of amino acids, TCA cycle metabolites and nucleotides (Fig. S9)
244 Moreover, whereas loss of either glucose or glutamine or both for 24 hours, strongly suppressed
245 mTORC1 signaling in non-adapted clones, adapted cells maintained significant mTORC1 activity even
246 in the absence of glucose, but particularly under low glutamine conditions (H-L or L-L). Similarly, GS
247 induction was highly dependent on both adaptation status and glutamine levels, with adapted clones
248 displaying highest GS protein levels under H-L or L-L conditions (Fig. S8*C*, with levels normalized and
249 quantified in *D*). This led us to investigate a possible genetic basis for induced mTORC1 activity in the
250 adapted clones and a potential role for mTORC1 in inducing GS levels under low glutamine conditions.
251
252 **mTORC1 activation and enhanced proliferative potential are reversible in adapted PDA clones**
253 Because the adapted clones sustain active mTORC1 signaling independent of nutrient deprivation, we
254 asked whether the adaptation process had selected for cells with inherent mutations that constitutively
255 activate mTORC1. We first cultured the SUIT-2 adapted clones in nutrient-replete H-H medium for 4 or
256 more consecutive passages (a process we termed "adaptation reversal") followed by treatment for 24
257 hours with L-L medium (Fig. 4*A*). Reverse-adapted (RA) clones displayed gradual suppression of
258 mTORC1 activity (Fig. 4*B*), indicating that the enhanced anabolic signaling acquired upon adaptation is
259 an unlikely result of genetic mutations selected for in the adapted clones. This was later confirmed with

260 Whole Exome Sequencing (WES) analysis that found no High or Moderate impact mutations (see
261 Methods) in any of the genes in the mTORC1 signaling pathway (Dataset S1) that was identified as
262 enriched at the transcriptional level, by GSEA (Fig. S4*G*). Indeed, of all 23 genes (Fig. S4*G*), only 10
263 genetic variants exist that were however found in all clones, independent of adaptation (C1-C9, Dataset
264 S1). Consistently, adapted and RA clones clustered according to clone number (Fig. S10*A*) rather than
265 according to adaptation, with no High impact mutations found in whole exome variants, implying that
266 genetic differences acquired upon reverse adaptation were minimal (Fig. S10*A* and Dataset S2).

267 Importantly, *in vitro* survival and growth of adapted clones were partially reversed, with all RA
268 clones exhibiting decreased proliferation compared to adapted clones, and one RA clone displaying a
269 trend in enhanced cell death (Fig. 4*C* and *D*). Furthermore, among a pool of 1,842 genes whose
270 expression was significantly altered (≥ 3-fold change, q <0.05) upon adaptation, about half of the
271 changes were partially reversed in RA clones (clusters I, II and V, Fig. 4*E*), consistent with decreased
272 mTORC1 signaling and proliferative capacity (Fig. 4*B* and *C*). These results imply that adaptation to
273 nutrient deprivation depends on a fraction of the transcriptional changes that accompany it.

274 Inactive gene regulatory elements tend to be inaccessible (closed chromatin), in contrast to active
275 cis-elements, which reside in open chromatin (32). To investigate a potential epigenetic basis for PDA
276 cells' adaptation to nutrient deprivation, we asked whether the transcriptional changes were associated
277 with chromatin dynamics. Assays for transposase-accessible chromatin with high throughput sequencing
278 (ATAC-seq) identified a significantly altered landscape of open chromatin in adapted clones, compared
279 to non-adapted clones, including gains and losses of chromatin accessibility near thousands of enhancers
280 (Fig. 4*F*). Adaptation-related increases in chromatin access correlated with increased mRNA levels and
281 conversely, reduced chromatin access correlated with lower mRNA levels (Fig. 4*G* and Fig. S10*B*).
282 Notably, alterations in open chromatin were largely preserved in reverse-adapted cells (Fig. 4*F* and Fig.

283 S10*C*, left) with infrequent reversion (Fig. 4*F* and Fig. S10*C*, right). Thus, most changes in chromatin
284 accessibility are stable, and again, adaptation depends only on a fraction of them. Further reversal of
285 open chromatin changes, with corresponding changes in gene expression and near complete reversal of
286 proliferative fitness, may require prolonged de-adaptation of PDA clones in nutrient-replete media.
287

288 **mTORC1 prevents proteasomal degradation of GS in adapted PDA clones**

289 Because the induction of GS protein in adapted cells consistently mirrored mTORC1 signaling (Fig. 2*C,*
290 3*B* and Fig. S8*B* and *C*), including reversibility upon de-adaptation (Fig. 4*B*), we asked whether
291 mTORC1 regulates GS levels. Upon treatment with the mTOR kinase inhibitor Torin1, *GS* mRNA
292 levels were increased in adapted clones under L-L conditions (Fig. S11*A*). In contrast, consistent with
293 post-transcriptional GS regulation, Torin1 markedly decreased GS protein levels (Fig. 5*A*). This
294 decrease was not observed upon treatment with cycloheximide, but only when Torin1 was added to the
295 cells, indicating that mTORC1 regulation of GS is post-translational (Fig. 5*B* and Fig. S11*B*). Indeed,
296 whereas treatment with the proteasomal inhibitor MG-132 did not significantly affect GS levels in
297 adapted clones over 2-8 hours, it induced GS at the 8-hour timepoint in non-adapted cells treated with L-
298 L media (Fig. 5*C*), despite suppressed activity of the translational regulator mTORC1 under these
299 conditions (Fig. 2*C*). Importantly, the Torin1-induced decrease in GS levels in adapted cells was rescued
300 upon treatment with MG-132 (Fig. 5*D*). Furthermore, mTORC1 inhibition promoted GS poly-
301 ubiquitination, as evidenced in immunoprecipitated GS from adapted cells co-treated with Torin1 and
302 MG-132 (Fig. 5*E*). Altogether, these data demonstrate that GS is ubiquitinated and targeted for
303 proteasomal degradation in non-adapted clones, even under L-L conditions, and that mTORC1 prevents
304 this degradation, leading to GS stabilization in adapted clones.
305

306 **PDA cells adapted to nutrient-deprived conditions are sensitive to GS inhibition**

307 To assess the contribution of glutamine synthesis to the enhanced growth of the adapted cells, PDA
308 clones were treated with the GS inhibitor L-methionine sulfoximine (MSO). Adapted cell proliferation
309 was mitigated under L-L, but not H-H conditions, underscoring the relevance of glutamine synthesis in
310 the nutrient-deprived state (Fig. S12*A*). Genetic silencing of GS similarly suppressed adapted cell
311 proliferation and colony formation (Fig. 6*A-C*, Fig. S12*B-D*). To ask whether the contribution of GS to
312 enhanced *in vitro* PDA growth extends *in vivo*, we induced knockdown of GS in orthotopic PDA
313 transplants (Fig. 6*D* and *E*). Five days following injection of adapted SUIT-2 cells expressing control or
314 *GS* hairpins into the pancreas, gene silencing was induced by treating mice with doxycycline (Dox) in
315 the drinking water. Two distinct *GS* hairpins attenuated PDA growth (Fig. 6*D* and Fig. S12*E* and *F*),
316 resulting in 6.1- to 9.2-fold lower tumor weights upon Dox treatment (Fig. 6*D*). Although no significant
317 changes in apoptosis were detected at the experimental endpoint, Ki-67 proliferative index tended to be
318 moderately lower in tumors upon GS knockdown (Fig. S12*G* and *H*). Altogether, our results indicate
319 that GS-mediated glutamine synthesis is required for PDA cells to survive and adapt to the characteristic
320 nutrient-deprived PDA environment and highlight GS as a metabolic target in treating pancreatic cancer
321 (Fig. 6*F*).

322 To extend our findings to human pathology, tissue microarrays (TMAs) of resected tumors from
323 127 pancreatic cancer patients were immunostained and scored for GS protein levels. As a reference for
324 intensity, stained control cores of normal pancreas showed high GS levels in islets and modest levels in
325 acinar cells. Within tumor cores, PDA cells displayed heterogeneous cytoplasmic staining that varied
326 widely from strong to moderate to weak, with an overall score lower than that of acinar cells. As a
327 result, no significant association was found between PDA GS levels and tumor size, lymph node
328 involvement (pT or pN staging, the American Joint Commission on Cancer, AJCC 8th edition (33)) or

329 patient survival (Fig. S13*A*-*C*). Although these results seem discordant with a recent report that GS
330 expression is a feature of *KRAS*-driven PDA (34), the pathological heterogeneity and variability in GS
331 protein levels is consistent with an inverse correlation with nutrient deprivation (Figs. 3, 4 and Fig. S8).
332 Indeed, nutrient distribution is recognized to be heterogeneous in the tumor microenvironment, with
333 glutamine levels being most depleted within tumor cores, compared to the periphery (19, 20). Therefore,
334 future studies could confirm whether gradients of GS protein levels exist among distinct PDA cell
335 clusters within the tumor mass, depending on their precise location and proximity to blood vessels.
336 Nevertheless, based on our results and those of Bott *et al.* (34), targeting GS in the nutrient-deprived
337 PDA tumors holds significant therapeutic value in pancreatic cancer.
338
339 **Discussion**
340 The *in vitro* dependence of proliferating cells on glutamine (22) was recently questioned in the *in vivo*
341 setting, where tumors preferably utilize glucose and other metabolites, rather than circulating glutamine,
342 as sources of tricarboxylic acid (TCA) cycle carbon (14, 35-37). This observation is supported by *in vivo*
343 resistance of tumors to inhibitors of glutaminolysis (38). Differences in nutrient levels between cell
344 culture media and human serum, in addition to the *in vivo* tumor environment, might partially explain
345 this discrepancy (12, 39). However, although glutamate is a major source of TCA cycle carbon and
346 nitrogen for transamination reactions and glutathione synthesis, glutamine *per se* is required for protein
347 synthesis and is an indispensable source of amide nitrogen for nucleotide and hexosamine synthesis
348 (34). Therefore, whereas proliferating tumor cells may resort to alternative sources of glutamate, such as
349 transamination reactions instead of glutaminolysis, they can only survive in glutamine-deprived
350 conditions if they can synthesize glutamine *de novo*.
351 Moreover, although glutamine may not seem to be depleted in extracts of whole tumors or tumor

352 interstitial fluid (16), tumor cores hold lower levels than the periphery (19, 20). Thus, the precise
353 location of a cancer cell within the hypoxic, stroma-dense tumor may dictate its dependence on
354 glutamine at various times. Distinct clusters of tumor cells likely exist within PDA tumors with
355 differential nutrient access depending on the proximity to blood vessels and density of the surrounding
356 stroma. The deprivation of PDA tumor cells of nutrients may also change over time, as tumor growth
357 reshapes 3D cellular organization and the proximity of cancer cells to stroma and endothelial cells. It is
358 therefore not surprising that, unlike Bott *et al.* (34), we found no significant association between average
359 GS levels and tumor grade or patient survival (Fig. S13). We find instead that rare clonal cells are able
360 to survive and adapt to low levels of the tumor-preferred nutrients glucose and glutamine; these cells
361 induce glutamine synthesis, which is required for their growth *in vitro* and *in vivo*.

362 Despite chronic nutrient deprivation in the adapted cells, we find that activated mTORC1
363 induces GS. Although GS is known to be regulated post-translationally (30, 31), the signaling basis for
364 this regulation was unknown. We show that mTORC1 plays a key post-translational role in stabilizing
365 GS by preventing its ubiquitination and proteasomal degradation. mTORC1 inhibition was previously
366 shown to enhance proteasomal degradation of long-lived proteins (40), but GS was not identified as a
367 specific target, perhaps because the experiments were performed under glutamine-replete conditions.
368 What induces mTORC1 activity in the absence of glucose and glutamine in adapted PDA cells is a
369 question worthy of future investigation. One plausible explanation is that epigenetic alterations that
370 occur upon adaptation to nutrient deprivation (Fig. 4 and Fig. S10) may influence genes that directly or
371 indirectly activate mTORC1 (Fig. S4*G*).

372 We propose that PDA cells that survive and adapt to nutrient deprivation acquire an epigenetic
373 state that endows them with the flexibility to switch between metabolic states that are optimal for growth
374 under nutrient-replete or nutrient-deprived conditions. A key contributing factor to the adaptation to

375 nutrient-depleted conditions is activation of mTORC1, which in turn stabilizes GS, thus enabling
376 essential glutamine synthesis for pancreatic cancer growth (Fig. 6*F*). Consequently, targeting of GS,
377 which expression is induced in nutrient-deprived cell clusters within PDA tumors, holds therapeutic
378 benefit to pancreatic cancer patients.
379
380 **Methods**
381 **Reagents.** Antibodies for western blotting were from Abcam: BCAT1 (ab107191), GOT2 /
382 FABP-1 (ab171739); BD Biosciences: GS / GLUL (BD-61057); Cell Signaling Technology
383 (CST): AKT (pan, C67E7, # 4691), pS473-AKT (193H12, # 4058), pT308-AKT (244F9, #
384 4056), BCAT2 (# 9432), CAD (# 11933), pS1859-CAD (# 12662), 4EBP1 (53H11, # 9644),
385 pS65-4EBP1 (# 9451), LC3B (# 2775), pThr389-S6K (# 9234); Novus Biologicals: GOT1
386 (NBP1-54778); Proteintech: GLUD1 / GDH1 (14299-1-AP); Santa Cruz Biotechnology: S6Kα
387 (H-9, sc-8418), GAPDH (FL-335, sc-25778), β-Actin (sc-47778). All western blot antibodies
388 were used at 1:1,000 dilution, except for β-Actin (1: 20,000). Antibodies for
389 immunoprecipitation, ubiquitination or immunohistochemistry are described in the respective
390 Methods sections below. Chloroquine (Sigma-Aldrich, C6628); Cycloheximide (Sigma-Aldrich,
391 C4859); DMSO (Sigma-Aldrich D2650); MG-132 (Selleck Chemicals, S2619); Doxycycline
392 (Sigma-Aldrich; D9891); L-Methionine Sulfoximine, MSO (Sigma-Aldrich; M5379); Torin 1
393 (Selleck Chemicals, S2827).
394
395 **Cell culture.** Human PDA cell lines were from the American Type Culture Collection or ATCC
396 (AsPC-1, BxPC-3, HPAC, MIA PaCa-2, PANC-1), Japanese Collection of Research
397 Bioresources (SUIT-2), or the German Collection of Microorganisms and Cell Cultures (PA-TU-

398 8988T) and were authenticated by STR profiling at ATCC. All cell lines tested negative for
399 mycoplasma using LookOut Mycoplasma PCR Kit (Sigma, MP0035). All cells were maintained
400 at 37°C in a humidified incubator with 5% CO2 and were grown in media supplemented with
401 10% dialyzed fetal bovine serum (Sigma-Aldrich F0392). For adaptation to "low glucose, low
402 glutamine" (L-L), "low glucose-high glutamine" (L-H), or "high glucose-low glutamine" (H-L),
403 PDA cells were cultured in RPMI 1640 medium lacking both glucose and L-glutamine (US
404 Biological, R9011-01) that was supplemented with either 0.5 mM glucose and 0.1 mM
405 glutamine for L-L; or with 0.5 mM glucose and 2mM glutamine (L-H); or with 11mM glucose,
406 0.1mM glutamine (H-L). Non-adapted cells were cultured in the same RPMI 1640 medium that
407 was however supplemented with 11mM glucose and 2 mM glutamine, and was termed "high
408 glucose, high glutamine" (H-H) medium. Glucose (A2494001) and glutamine (25030-81)
409 were from Thermo Fisher Scientific.
410
411 **Gene knockdown.** For small interfering RNA knockdown, ON-TARGETplus Human GS
412 (GLUL) siRNA with target sequence: GCACACCUGUAAACGGAUA (J-008228-09) or control
413 non-targeting siRNA: UGGUUUACAUGUUGUGUGA (D-001810-02-05) were purchased from
414 Dharmacon, Horizon Discovery (Cambridge, UK) and transfected according to the
415 manufacturer's protocol. For generation of PDA cells with stable doxycycline-inducible GS or
416 control (Scramble) knockdown, hairpins were cloned into Tet-pLKO-puro plasmid (21915;
417 Addgene). Lentiviral supernatants were generated by transfecting the plasmids into 293T cells
418 and used to infect 8988T cells that were then selected for at least 7 days with 2 μg ml^{-1}
419 puromycin (Sigma-Aldrich, P8833). The RNAi consortium clone IDs for the hairpins used were:
420 shGS #1 (G05) TRCN0000343992 (CACACCTGTAAACGGATAATG); shGS #2 (G06)

421 TRCN0000344059 (ATAACCACTGCTTCCATTTAA); Control Scramble shRNA sequence
422 (CCTAAGGTTAAGTCGCCCTCGCTCGAGCGAGGGCGACTTAACCTTAGG) was the
423 same as that from Addgene Plasmid # 1864.
424
425 **Cell proliferation and cell death assays.** Cells were seeded on day 0 in their respective
426 maintenance culture medium in 96-well plates, at a density of 3,000 cells per well, and incubated
427 overnight. On day 1, the cells were washed once with phosphate buffered saline (PBS) and
428 incubated, without replenishment, in their experimental medium supplemented with propidium
429 iodide (2 $\mu g\ ml^{-1}$) for up to 7 days. Live or dead cells (propidium iodide-negative or -positive,
430 respectively) were counted on the indicated days using the Celigo Image Cytometer (Nexcelom
431 Bioscience), and either normalized to day 1 (live cell proliferation curves), or presented as
432 percentage of propidium iodide-positive cells per total cell number (cell death).
433
434 **Clonogenic assay.** 600 cells were seeded per well in 6-well plates in their appropriate
435 maintenance medium and incubated overnight. The next day, cells were washed once with PBS
436 and incubated in their experimental medium for 7-10 days. Colonies were then either directly
437 counted using the Celigo Image Cytometer (Nexcelom Bioscience), or first stained and then
438 counted using the following protocol: media were removed and the cells fixed in a solution of
439 0.2% Crystal Violet (Sigma-Aldrich, C0775) in 80% methanol for 15-30 min. The wells were
440 then washed in distilled water and allowed to dry overnight, before colonies were counted using
441 the Celigo Image Cytometer.
442

443 **Sphere formation assay.** 50 cells were seeded per well in 96-well plates and incubated
444 overnight in their appropriate maintenance medium supplemented with 4% matrigel (Corning,
445 356231). The next day, cells were washed once gently with PBS and treated with the
446 experimental medium. Spheres were counted after 7-10 days using the Celigo Image Cytometer
447 (Nexelcom Bioscience).
448
449 **Macropinocytosis assay.** Cells were seeded onto glass coverslips (Bellco Glass, 1943-10012A)
450 in 24-well plates and incubated overnight in their maintenance culture medium. The next day, the
451 medium was replaced with fresh L-L medium containing 10% dialyzed FBS, and the cells were
452 incubated for 24 h. Macropinosomes were assayed as previously described (41) and outlined
453 below. 70-kDa TMR-dextran (Thermo Fisher Scientific, D1818) was added to the cells at a final
454 concentration of 1 mg ml^{-1} and the cells incubated for 30 min at 37°C, in the absence or presence
455 of 25 μM EIPA (Sigma-Aldrich; A3085). Cells were then rinsed 3 times on ice with ice-cold
456 PBS and immediately fixed in 4% paraformaldehyde (EMS, 15710-S) for 30 min. After staining
457 the cells with 1 μg ml^{-1} DAPI (Thermo Scientific, D3571) in PBS for 15min, the coverslips were
458 mounted onto glass slides (VWR, 48311-703) using Fluoroshield mounting medium (Sigma,
459 F6182). Image acquisition was performed using a Nikon Eclipse 90i Advanced Automated
460 Research Microscope equipped with a standard optical filter set including DAPI and
461 Rhodamine/Texas Red. Images were captured with a 40x objective and the NIS-Elements
462 Advanced Research Microscope Imaging Software (Nikon). Exposure time for DAPI acquisition
463 was 100 ms and that for TMR acquisition was 400 ms. Representative images were captured in
464 at least 3 different fields per well in duplicate wells, per condition and analyzed using ImageJ
465 software (NIH). At least 200 cells were counted per condition. Macropinosomes were visualized

466 after setting the threshold of the "Auto Contrast" feature in Image J to 134. The number and area
467 of labeled macropinosomes were then determined using the "Analyze Particles" feature, and
468 macropinocytic uptake was computed by the total particle number and area per cell.
469
470 **U-^{14}C-asparate incorporation into DNA**
471 Cells were seeded overnight (57,000 per well) in 6-well-plates with triplicate wells per condition.
472 The cells were then washed twice with PBS and incubated with either H-H or L-L medium
473 supplemented with 1μCi per well of L-[U-^{14}C]-Aspartic acid (PerkinElmer,
474 NEC268E050UC) for 40 h. The cells were washed twice with PBS before DNA was extracted
475 using PureLink® Genomic DNA Mini Kit (Thermo Fisher-K182001) and quantified using a
476 spectrophotometer. Equal volumes of DNA were added to scintillation vials and radioactivity
477 was measured by liquid scintillation counting and normalized to total DNA concentration.
478
479 **Immunoblotting.** For western blotting, cells were rinsed once in ice-cold PBS and collected in
480 lysis buffer containing 50 mM HEPES KOH, pH 7.4, 40mM NaCl, 2mM EDTA, 1.5mM
481 orthovanadate, 50mM NaF, 10mM pyrophosphate, 10mM glycerophosphate, EDTA-free
482 protease inhibitors (Thermo Fisher Scientific, 88266) and 1% Triton X-100. Proteins from total
483 lysates were resolved by 8–12% SDS–PAGE, transferred to polyvinylidene difluoride (PVDF)
484 and the blot was exposed to film.
485
486 **Immunoprecipitation and ubiquitination assay.** To assess GS protein ubiquitination, cells
487 were treated with either control vehicle DMSO or MG132 (10 μM) for 8 h. Cells were then lysed
488 under denaturing conditions using the lysis buffer (40 mM HEPES KOH, pH 7.4, 1% SDS)

489 containing 5 mM N-ethylmaleimide (NEM, Sigma-Aldrich, E1275) to prevent deubiquitination
490 and boiled for 5 min. The lysates were diluted 10-fold in IP buffer (40 mM HEPES KOH pH 7.4,
491 50 mM NaF, 10 mM Sodium pyrophosphate, 10 mM Sodium beta-glycerophosphate, 1.5 mM
492 Sodium Orthovanadate, 2.5 mM MgCl2, EDTA-free protease inhibitors, and 0.5% Triton X-
493 100). IP was performed by incubating the samples with 2 μg of normal rabbit IgG control (Santa
494 Cruz, sc-2027) or 2μg GS antibody (Abcam, ab73593) overnight with rotation at 4°C. Protein G
495 agarose bead slurry (Invitrogen, 15920-010) was added to the pre-cleared lysates (60 μl, 50:50)
496 and incubated with rotation for 1.5-2 hr at 4°C. The beads were then washed once with IP buffer,
497 followed by 3 additional washes with IP buffer supplemented with 500 mM NaCl. Loading
498 buffer was added to the immunoprecipitated proteins, which were then boiled, resolved by SDS-
499 PAGE and transferred to a PVDF membrane. Ubiquitinated GS was identified by HRP-
500 conjugated anti-Ubiquitin antibody (1:5,000; Enzo Life Sciences, FK2, BML-PW0150-0100).
501
502 **Quantitative real-time PCR.** Total mRNA was isolated with RNA STAT-60 (Tel-Test, Cs-111)
503 according to the manufacturer's instructions, treated with DNase I (RNase-free, Roche
504 Molecular Biochemicals**,** 04716728001) and reverse-transcribed into cDNA with random
505 hexamers using the SuperScript II First-Strand Synthesis System (Invitrogen, 18064071).
506 Primers listed below were validated and PCR reactions performed as previously described (42).
507 Quantitative PCR reactions were performed in triplicates using an Applied Biosystems ViiA 7
508 Real-Time PCR system. PCR reactions contained cDNA resulting from reverse transcription of
509 25ng total RNA, 150nM of each primer and 5 μl 2X-Jump Start SYBR Green PCR Mix
510 (Invitrogen) in10 μl total volume. Relative mRNA levels were calculated using the comparative
511 CT method and normalized to cyclophilin. The QPCR primers used were:

512 *CyclophilinA* (CYPA): 5'-GGAGATGGCACAGGAGGAA-3' and 5'-
513 GCCCGTAGTGCTTCAGCTT-3'
514 *GS*: 5'-AAGAGTTGCCTGAGTGGAATTTC-3' and 5'-AGCTTGTTAGGGTCCTTACGG-3'**.**
515
516 **RNA-Seq sample preparation**: Cells were seeded overnight at 700,000 per 10 cm plate. The
517 cells were then washed once with PBS and incubated in L-L medium for 24 h. RNA was
518 isolated and purified using miRNeasy Mini Kit (Qiagen-217004). Total RNA (> 150 ng) was
519 sent to the Broad Institute Genomics Platform for library preparation. RNA quality and insert-
520 size was assessed by Caliper LabchipGXII producing a RQS value (equivalent to RIN). RNA
521 quantity was determined by PicoGreen. mRNA libraries were prepared using the Illumina
522 TruSeq Stranded mRNA kit modified for improved performance and multiplexing. Libraries
523 were pooled and sequenced with the Illumina HiSeq 4000 using 101-cycle, pair-end settings to
524 obtain 50 million read sequencing depth per sample.
525
526 **RNA read processing and Quantification.** All samples were processed using an RNA-Seq
527 pipeline implemented in the bcbio-nextgen project (https://bcbio-
528 nextgen.readthedocs.io/en/latest/). Raw reads were examined for quality issues using FastQC
529 (http://www.bioinformatics.babraham.ac.uk/projects/fastqc/) to ensure library generation and
530 sequencing data were suitable for further analysis. Reads were aligned to the hg19 build of
531 the human genome using STAR(43). Quality of alignments was assessed by checking for
532 evenness of coverage, rRNA content, genomic context of alignments, complexity and other
533 quality checks. Expression quantification was performed with Salmon(44) to identify transcript-
534 level abundance estimates and then collapsed down to the gene-level using the R Bioconductor

535 package tximport (45). Differential expression was performed at the gene level using the R
536 Bioconductor package DESeq2(46). Differentially expressed genes were identified using the
537 Wald test and significant genes were obtained using an FDR threshold of 0.05. GSEA(47) was
538 carried out on the full expression data matrix using the gene sets collection from Kyoto
539 Encyclopedia of Genes and Genomes (KEGG) to assess the enrichment of the "adaptation to
540 nutrient deprivation" signature. A pairwise GSEA (v4.1.0) was performed by creating ranked
541 lists of genes using the difference of class means to calculate fold change for log scale data
542 between the Adapted and Non-Adapted PDA clones (Fig. S4) and *P* values were obtained from
543 permuting the gene set (1000 permutations).
544
545 **ATAC-Seq.** Cells were seeded overnight at 700,000 per 10 cm plate, washed once with PBS,
546 and incubated in L-L medium for 24 h. The assay (48) was performed on 10^6 cells per condition.
547 Cells were washed twice in ice-cold PBS and resuspended in 50 μl ice-cold ATAC lysis buffer
548 (10 mM Tris.Cl, pH 7.4, 10 mM NaCl, 3 mM $MgCl_2$, 0.1% (v/v) Igepal CA-630), and
549 centrifuged at 500 g at 4°C to isolate nuclear pellets that were treated in 50 μL reactions with
550 Nextera Tn5 Transposase (Illumina, FC-121-1030) for 30 min at 37°C. Column-purified DNA
551 (QIAGEN) was stored at 20°C or amplified immediately in 50 μl reactions with high-fidelity 2X
552 PCR Master Mix (New England Biolabs) using a common forward primer and different reverse
553 primers with unique barcodes for each sample. From the reaction mix, 45 μl was kept on ice after
554 5 cycles of PCR, while 5 μl was amplified by qPCR for 20 additional cycles; the remaining 45 μl
555 was then amplified for the 5-7 cycles required to achieve 1/3 of the maximum qPCR
556 fluorescence intensity. Amplified DNA was purified over columns and primer dimers (<100 bp)
557 were removed using AMPure beads (Beckman Coulter). Size distribution of the amplified DNA

558 was analyzed using High-sensitivity Qubit dsDNA Assay Kit (ThermoFisher). High throughout
559 sequencing was performed by Novogene Corporation, Inc. (Sacramento, CA). Computational
560 analysis was performed as described previously (49).
561
562 **Whole Exome Sequencing (WES).** Cells were seeded overnight at 700,000 per 10 cm plate,
563 then washed once with PBS and incubated in L-L medium for 24 h. DNA was isolated and
564 purified using Genomic DNA Mini Kit (Invitrogen, K-1820-01). Library preparation (Agilent
565 SureSelect Human All Exon V6 kit) and high throughout sequencing (Illumina NovaSeq 6000,
566 pair-end, 100 X coverage), were performed by Novogene Corporation, Inc. (Sacramento, CA).
567 Variants were called in 9 WES samples: SUIT-2 non-adapted (C1-C3), adapted (C4-C6) or
568 reverse-adapted (C4-C5) clones in a single batch using HaplotypeCaller in gatk4.1.4.1 (50) as
569 implemented in bcbio-nextgen variant2 pipeline (https://doi.org/10.5281/zenodo.3564938). Main
570 steps of the pipeline included: read alignment with bwa mem (51), bam file processing with
571 samtools (52) and sambamba (53), quality control with multiqc (54), coverage analysis with
572 mosdepth (55), variant annotation with snpEff (56) and vcfanno (57). Gnomad database was
573 used as annotation resource for variant population frequencies (58). High and Moderate impact
574 variants were defined according to snpEff documentation. High impact variants include stop-
575 gain, frameshift and splice site variants. Moderate impact variants include mostly missense
576 variants. For mTOR signaling pathway: variant calling resulted in 213,965 variants with read
577 depth > 50 across 9 samples. Variants were filtered for High and Moderate impact, yielding
578 17,226 variants, 10 of which are located in the 23 genes from the mTOR pathway list in Figure
579 S4*G*. All variants in mTOR pathway genes were shared between all 9 samples, none of the
580 variants segregated according to adaptation phenotype (Dataset S1).

581 For all genes: Variants of High or Moderate impact were selected, rare in human population
582 (gnomad AF < 1%), and absent at least in one sample. Variants present in all samples were
583 removed. This resulted in 581 variants, 117 of which were of High impact (Dataset S2, sheets 1
584 and 2). High impact samples were clustered based on the presence or absence of High variants
585 (Fig. S10*A*). Clustering was performed using R, r-studio, using ggplot2 and tidyverse packages,
586 ggdendro, cowplot and hclust.
587
588 **Metabolite tracing, extraction and quantification.** For stable isotope tracing experiments, cells
589 were incubated for 24 h in L-L or H-H medium supplemented with either 0.8mM ^{15}N-
590 ammonium chloride (99% enrichment, NLM-467-1) or 0.4mM ^{15}N-leucine (98% enrichment,
591 NLM-142-0.5) purchased from Cambridge Isotope Laboratories. Cells were then rinsed in ice-
592 cold PBS and metabolites extracted with ice-cold 80% methanol, vortexed for 10min at 4°C, and
593 centrifuged at top speed (10min, 10,000 x g, 4°C). Supernatants were transferred to fresh
594 Eppendorf tubes and dried using a SpeedVac. Dried extracts were suspended in 100 µl water and
595 centrifuged at top speed for 10 min, and the supernatant was analyzed using LC-MS. For Figures
596 2*A*, 3*C*, 3*E*, and S5, data analysis and natural abundance correction of the stable isotope labeling
597 data were performed as previously described (59). For Figures 3*F* and S9, data were acquired
598 using a hydrophilic interaction liquid chromatography (HILIC)-positive ion mode mass
599 spectrometry (MS) method operated on Nexera X2 UHPLC (Shimadzu Scientific Instruments,
600 Marlborough, MA) coupled to a Q Exactive orbitrap mass spectrometer (Thermo Fisher
601 Scientific, Waltham, MA) as described previously (60), with full scan high resolution MS data
602 collected over 70–800 m/z. For global steady-state metabolite profiling, data were analyzed
603 using MetaboAnalyst 4.0 (61), median-normalized, log-transformed, mean-centered and divided

604 by the S.D. of each variable. For heatmaps, the intensity of the red or blue color varies depending
605 on the number of groups included in a specific analysis (e.g. Fig. 2*A* and Fig. 3*E*, compared to
606 Fig. S5*A*). This is because the intensity reflects the relative levels of each metabolite among all
607 groups, rather than its absolute levels. Nevertheless, increased or decreased metabolite levels
608 between any 2 groups remain evident.
609
610 **Animal work.** All mouse studies and procedures were approved by the Animal Care and Use
611 Committee at Boston Children's Hospital. For orthotopic xenografts, 750 x 10^3 cells suspended
612 in 25 µl 33% Matrigel (Corning, 356231) in Hank's Balanced Salt Solution (HBSS) were
613 injected into the pancreata of male B6.129S7-$Rag^{1tm1Mom}$/J mice termed $Rag1^{-/-}$ mice (Jackson
614 Laboratory #002216). *In vivo* ultrasound imaging (Vevo 2100, MS550D Scanhead) was
615 performed on mice to detect and quantify tumor growth at the Small Animal Imaging Lab
616 (SAIL) at Boston Children's Hospital. Following experimental endpoint euthanasia, tumors
617 were collected, their dimensions (**a**, **b** and **c**) were measured with a caliper and tumor volume
618 was estimated according to the ellipsoid formula(62): 4/3 x π x (a/2 x b/2 x c/2). Tumor tissue
619 was then either immediately frozen in liquid nitrogen, or fixed in formalin for later processing.
620
621 **Immunohistochemistry and analysis of human samples.** Formalin-fixed paraffin-embedded
622 murine PDA tumors were sectioned and stained with Hematoxylin and Eosin (H&E), Ki-67 (BD
623 Biosciences, #550609) or cleaved caspase 3 (CST, #9664). Human PDA tissue microarrays
624 (TMAs) with 2–3 cores per case, were sectioned and immunostained with GS antibody (abcam,
625 ab-73593). Immunostaining was performed according to the manufacturer's protocol. A
626 pathologist scored, in a blinded fashion, the intensity of staining on a scale of 0-3 that

627 represented none (0), weak (1), moderate (2), or strong (3) based on the PDA cell staining.
628 Scores for each tumor core were estimated using the following formula: H-score = 0 x (% area of
629 tumor with no staining) + 1 x (% tumor area with weak staining) + 2 x (% tumor area with
630 moderate staining) + 3 x (% tumor area with strong staining), where 300 would be the highest
631 score. TMAs were derived from 127 patients with surgically resected PDA from Massachusetts
632 General Hospital. Informed patient consent was waived by the Institutional Review Board or
633 IRB (Protocol Number 2009P001838), as the TMAs were generated from discarded material
634 following clinical diagnosis. For analyses of human data, the following variables were from
635 electronic medical records: age, sex, pN and pT stage based on the American Joint Committee on
636 Cancer 8th edition, tumor size, location and grade of differentiation, and presence of
637 lymphovascular and perineural invasion. Survival analyses were performed using overall
638 survival (OS) as the outcome of interest, defined as the time between surgical resection and death
639 from any cause or date of last clinical contact. Survival outcomes were compared based on
640 tertiles of GS staining intensity as assessed by H-scores using the Kaplan-Meier method. Tertile
641 thresholds were 115 and 150 H-score units. As secondary analyses, GS intensity was evaluated
642 for its association with baseline clinicopathological characteristics at the time of surgery using
643 the Kruskal-Wallis test. Statistical significance was set at $P < 0.05$. Data analysis was performed
644 using SAS 9.4 (version 9.4, SAS Institute, Cary, NC).
645
646 **Statistical Analysis**
647 Data were presented as mean ± S.D. or ± S.E.M., unless otherwise indicated. When comparing
648 two groups, a two-tailed non-paired Student's t-test was conducted. For three or more groups,
649 one-way ANOVA (for one factor) or two-way ANOVA (2 factors) was conducted. ANOVA was

650 followed by post hoc Tukey's multiple-comparison test. $p < 0.05$ was considered statistically
651 significant.
652
653 **Acknowledgements**
654 We thank members of the Kalaany lab and the Division of Endocrinology for helpful
655 comments and discussions. This work was supported by the American Cancer Society
656 Research Scholar Grant (RSG-17-070-01-TBG) to N.Y.K. and funds from Boston Children's
657 Hospital. N.Y.K. is also supported by NIH/NCI Grant R01 CA211944. P-Y.T. was partly
658 funded by Top University Strategic Alliance (TUSA) fellowship from Taiwan. Work by M.M.
659 and S.N. was supported by Harvard Catalyst, The Harvard Clinical and Translational Science
660 Center (NIH award #UL1 RR 025758) and computations were run on the Orchestra cluster
661 supported by HMS Research Computing Group.
662
663 **Author Contributions**
664 N.Y.K. conceived, designed and supervised the study. P-Y.T. and M-S.L. performed all
665 experiments with help from lab members and collaborators. M-S.L. performed biochemical
666 assays for GS stabilization and growth assays for stable GS knockdown with help from I.N. who
667 also assisted in macropinocytosis quantification and western blotting. A.A. assisted P-Y.T. with
668 tumor cell injection into mice. M.M. analyzed RNA-Seq data and M-S.L. performed pathway
669 analyses (Fig. S4). S.N. performed WES analysis. R.A.M. supervised the ATAC-Seq experiment
670 and analyses, contributing to the interpretation of the results. U.J. performed the ATAC-Seq
671 assay and analyzed the ATAC-Seq and RNA-Seq data (Fig. 4*E*-*G* and Fig. S10*B* and *C*) with
672 help from S.M. C.A.L. performed metabolite quantification and tracing analyses (Figs 2*A* and 3*C*

673 and *E* and Fig. S5). D.S.H., with supervision from C.B.C., performed metabolite quantification
674 and tracing analyses (Fig. 3*F* and Fig. S9). F.R.R. assisted with mouse ultrasound imaging.
675 M.M.-K. provided TMAs and pathological assessment and scoring for immunostained human
676 pancreatic tissue. T.H. and K.C.H. helped retrieve patient data. P.D. performed the statistical
677 analyses on human data with consultation from V.M.-O. who contributed to the discussion of the
678 results. N.Y.K., P.-Y.T. and M-S.L. wrote the manuscript with feedback from all authors.
679

680 **Supplementary information**

681 Supplementary Figures S1-13 and Datasets S1 and S2 accompany this manuscript.
682

683 **Data availability**

684 The RNA-Seq, ATAC-Seq and DNA-Seq (WES) data have been deposited in NCBI's Gene
685 Expression Omnibus and are accessible through GEO Series accession number GSE144833.
686

687 **Competing interests**

688 The authors declare no competing financial interests.
689

690 **References**

691 1. R. L. Siegel, K. D. Miller, A. Jemal, Cancer statistics, 2019. *CA Cancer J Clin* **69**, 7-34
692 (2019).
693 2. L. Rahib *et al.*, Projecting cancer incidence and deaths to 2030: the unexpected burden of
694 thyroid, liver, and pancreas cancers in the United States. *Cancer Res* **74**, 2913-2921
695 (2014).
696 3. R. M. Perera, N. Bardeesy, Pancreatic Cancer Metabolism: Breaking It Down to Build It
697 Back Up. *Cancer Discov* **5**, 1247-1261 (2015).
698 4. H. Ying *et al.*, Genetics and biology of pancreatic ductal adenocarcinoma. *Genes Dev* **30**,
699 355-385 (2016).

700 5. S. Yang *et al.*, Pancreatic cancers require autophagy for tumor growth. *Genes Dev* **25**,
701 717-729 (2011).
702 6. C. Commisso *et al.*, Macropinocytosis of protein is an amino acid supply route in Ras-
703 transformed cells. *Nature* **497**, 633-637 (2013).
704 7. J. J. Kamphorst *et al.*, Human pancreatic cancer tumors are nutrient poor and tumor cells
705 actively scavenge extracellular protein. *Cancer Res* **75**, 544-553 (2015).
706 8. O. Olivares *et al.*, Collagen-derived proline promotes pancreatic ductal adenocarcinoma
707 cell survival under nutrient limited conditions. *Nat Commun* **8**, 16031 (2017).
708 9. H. Ying *et al.*, Oncogenic Kras maintains pancreatic tumors through regulation of
709 anabolic glucose metabolism. *Cell* **149**, 656-670 (2012).
710 10. J. Son *et al.*, Glutamine supports pancreatic cancer growth through a KRAS-regulated
711 metabolic pathway. *Nature* **496**, 101-105 (2013).
712 11. A. Muir, M. G. Vander Heiden, The nutrient environment affects therapy. *Science* **360**,
713 962-963 (2018).
714 12. S. M. Davidson *et al.*, Environment Impacts the Metabolic Dependencies of Ras-Driven
715 Non-Small Cell Lung Cancer. *Cell Metab* **23**, 517-528 (2016).
716 13. C. T. Hensley *et al.*, Metabolic Heterogeneity in Human Lung Tumors. *Cell* **164**, 681-694
717 (2016).
718 14. E. A. Maher *et al.*, Metabolism of [U-13 C]glucose in human brain tumors in vivo. *NMR*
719 *Biomed* **25**, 1234-1244 (2012).
720 15. I. Marin-Valencia *et al.*, Analysis of tumor metabolism reveals mitochondrial glucose
721 oxidation in genetically diverse human glioblastomas in the mouse brain in vivo. *Cell*
722 *Metab* **15**, 827-837 (2012).
723 16. M. R. Sullivan *et al.*, Quantification of microenvironmental metabolites in murine
724 cancers reveals determinants of tumor nutrient availability. *Elife* **8** (2019).
725 17. J. R. Cantor *et al.*, Physiologic Medium Rewires Cellular Metabolism and Reveals Uric
726 Acid as an Endogenous Inhibitor of UMP Synthase. *Cell* **169**, 258-272 e217 (2017).
727 18. J. Vande Voorde *et al.*, Improving the metabolic fidelity of cancer models with a
728 physiological cell culture medium. *Sci Adv* **5**, eaau7314 (2019).
729 19. M. Pan *et al.*, Regional glutamine deficiency in tumours promotes dedifferentiation
730 through inhibition of histone demethylation. *Nat Cell Biol* **18**, 1090-1101 (2016).
731 20. S. W. Lee *et al.*, EGFR-Pak Signaling Selectively Regulates Glutamine Deprivation-
732 Induced Macropinocytosis. *Dev Cell* 10.1016/j.devcel.2019.05.043 (2019).
733 21. N. Psychogios *et al.*, The human serum metabolome. *PLoS One* **6**, e16957 (2011).
734 22. B. J. Altman, Z. E. Stine, C. V. Dang, From Krebs to clinic: glutamine metabolism to
735 cancer therapy. *Nat Rev Cancer* **16**, 749 (2016).
736 23. T. Gebregiworgis *et al.*, Glucose Limitation Alters Glutamine Metabolism in MUC1-
737 Overexpressing Pancreatic Cancer Cells. *J Proteome Res* **16**, 3536-3546 (2017).
738 24. H. W. S. Tan, A. Y. L. Sim, Y. C. Long, Glutamine metabolism regulates autophagy-
739 dependent mTORC1 reactivation during amino acid starvation. *Nat Commun* **8**, 338
740 (2017).
741 25. L. Yan, P. Raj, W. Yao, H. Ying, Glucose Metabolism in Pancreatic Cancer. *Cancers*
742 *(Basel)* **11** (2019).
743 26. I. Ben-Sahra, J. J. Howell, J. M. Asara, B. D. Manning, Stimulation of de novo
744 pyrimidine synthesis by growth signaling through mTOR and S6K1. *Science* **339**, 1323-
745 1328 (2013).

746 27. L. S. Harrington *et al.*, The TSC1-2 tumor suppressor controls insulin-PI3K signaling via
747 regulation of IRS proteins. *J Cell Biol* **166**, 213-223 (2004).
748 28. P. P. Hsu *et al.*, The mTOR-regulated phosphoproteome reveals a mechanism of
749 mTORC1-mediated inhibition of growth factor signaling. *Science* **332**, 1317-1322
750 (2011).
751 29. O. J. Shah, Z. Wang, T. Hunter, Inappropriate activation of the TSC/Rheb/mTOR/S6K
752 cassette induces IRS1/2 depletion, insulin resistance, and cell survival deficiencies. *Curr*
753 *Biol* **14**, 1650-1656 (2004).
754 30. T. V. Nguyen *et al.*, Glutamine Triggers Acetylation-Dependent Degradation of
755 Glutamine Synthetase via the Thalidomide Receptor Cereblon. *Mol Cell* **61**, 809-820
756 (2016).
757 31. T. V. Nguyen *et al.*, p97/VCP promotes degradation of CRBN substrate glutamine
758 synthetase and neosubstrates. *Proc Natl Acad Sci U S A* **114**, 3565-3571 (2017).
759 32. S. L. Klemm, Z. Shipony, W. J. Greenleaf, Chromatin accessibility and the regulatory
760 epigenome. *Nat Rev Genet* **20**, 207-220 (2019).
761 33. P. J. Allen *et al.*, Multi-institutional Validation Study of the American Joint Commission
762 on Cancer (8th Edition) Changes for T and N Staging in Patients With Pancreatic
763 Adenocarcinoma. *Ann Surg* **265**, 185-191 (2017).
764 34. A. J. Bott *et al.*, Glutamine Anabolism Plays a Critical Role in Pancreatic Cancer by
765 Coupling Carbon and Nitrogen Metabolism. *Cell Rep* **29**, 1287-1298 e1286 (2019).
766 35. M. O. Yuneva *et al.*, The metabolic profile of tumors depends on both the responsible
767 genetic lesion and tissue type. *Cell Metab* **15**, 157-170 (2012).
768 36. S. Tardito *et al.*, Glutamine synthetase activity fuels nucleotide biosynthesis and supports
769 growth of glutamine-restricted glioblastoma. *Nat Cell Biol* **17**, 1556-1568 (2015).
770 37. S. H. Issaq, A. Mendoza, S. D. Fox, L. J. Helman, Glutamine synthetase is necessary for
771 sarcoma adaptation to glutamine deprivation and tumor growth. *Oncogenesis* **8**, 20
772 (2019).
773 38. D. E. Biancur *et al.*, Compensatory metabolic networks in pancreatic cancers upon
774 perturbation of glutamine metabolism. *Nat Commun* **8**, 15965 (2017).
775 39. A. Muir *et al.*, Environmental cystine drives glutamine anaplerosis and sensitizes cancer
776 cells to glutaminase inhibition. *Elife* **6** (2017).
777 40. J. Zhao, B. Zhai, S. P. Gygi, A. L. Goldberg, mTOR inhibition activates overall protein
778 degradation by the ubiquitin proteasome system as well as by autophagy. *Proc Natl Acad*
779 *Sci U S A* **112**, 15790-15797 (2015).
780 41. C. Commisso, R. J. Flinn, D. Bar-Sagi, Determining the macropinocytic index of cells
781 through a quantitative image-based assay. *Nat Protoc* **9**, 182-192 (2014).
782 42. A. L. Bookout, D. J. Mangelsdorf, Quantitative real-time PCR protocol for analysis of
783 nuclear receptor signaling pathways. *Nucl Recept Signal* **1**, e012 (2003).
784 43. A. Dobin *et al.*, STAR: ultrafast universal RNA-seq aligner. *Bioinformatics* **29**, 15-21
785 (2013).
786 44. R. Patro, G. Duggal, M. I. Love, R. A. Irizarry, C. Kingsford, Salmon provides fast and
787 bias-aware quantification of transcript expression. *Nat Methods* **14**, 417-419 (2017).
788 45. C. Soneson, M. I. Love, M. D. Robinson, Differential analyses for RNA-seq: transcript-
789 level estimates improve gene-level inferences. *F1000Res* **4**, 1521 (2015).
790 46. M. I. Love, W. Huber, S. Anders, Moderated estimation of fold change and dispersion for
791 RNA-seq data with DESeq2. *Genome Biol* **15**, 550 (2014).

792 47. A. Subramanian *et al.*, Gene set enrichment analysis: a knowledge-based approach for
793 interpreting genome-wide expression profiles. *Proc Natl Acad Sci U S A* **102**, 15545-
794 15550 (2005).
795 48. J. D. Buenrostro, B. Wu, H. Y. Chang, W. J. Greenleaf, ATAC-seq: A Method for
796 Assaying Chromatin Accessibility Genome-Wide. *Curr Protoc Mol Biol* **109**, 21 29 21-
797 29 (2015).
798 49. U. Jadhav *et al.*, Dynamic Reorganization of Chromatin Accessibility Signatures during
799 Dedifferentiation of Secretory Precursors into Lgr5+ Intestinal Stem Cells. *Cell Stem Cell*
800 **21**, 65-77 e65 (2017).
801 50. A. McKenna *et al.*, The Genome Analysis Toolkit: a MapReduce framework for
802 analyzing next-generation DNA sequencing data. *Genome Res* **20**, 1297-1303 (2010).
803 51. H. Li, Aligning sequence reads, clone sequences and assembly contigs with BWA-MEM.
804 *arXiv.org* 1303.3997 (2013).
805 52. H. Li *et al.*, The Sequence Alignment/Map format and SAMtools. *Bioinformatics* **25**,
806 2078-2079 (2009).
807 53. A. Tarasov, A. J. Vilella, E. Cuppen, I. J. Nijman, P. Prins, Sambamba: fast processing of
808 NGS alignment formats. *Bioinformatics* **31**, 2032-2034 (2015).
809 54. P. Ewels, M. Magnusson, S. Lundin, M. Kaller, MultiQC: summarize analysis results for
810 multiple tools and samples in a single report. *Bioinformatics* **32**, 3047-3048 (2016).
811 55. B. S. Pedersen, A. R. Quinlan, Mosdepth: quick coverage calculation for genomes and
812 exomes. *Bioinformatics* **34**, 867-868 (2018).
813 56. P. Cingolani *et al.*, A program for annotating and predicting the effects of single
814 nucleotide polymorphisms, SnpEff: SNPs in the genome of Drosophila melanogaster
815 strain w1118; iso-2; iso-3. *Fly (Austin)* **6**, 80-92 (2012).
816 57. B. S. Pedersen, R. M. Layer, A. R. Quinlan, Vcfanno: fast, flexible annotation of genetic
817 variants. *Genome Biol* **17**, 118 (2016).
818 58. K. J. Karczewski *et al.*, The mutational constraint spectrum quantified from variation in
819 141,456 humans. *Nature* **581**, 434-443 (2020).
820 59. N. Kanarek *et al.*, Histidine catabolism is a major determinant of methotrexate sensitivity.
821 *Nature* **559**, 632-636 (2018).
822 60. I. D. Mascanfroni *et al.*, Metabolic control of type 1 regulatory T cell differentiation by
823 AHR and HIF1-alpha. *Nature medicine* **21**, 638-646 (2015).
824 61. J. Chong, D. S. Wishart, J. Xia, Using MetaboAnalyst 4.0 for Comprehensive and
825 Integrative Metabolomics Data Analysis. *Curr Protoc Bioinformatics* **68**, e86 (2019).
826 62. I. L. Wapnir, D. E. Wartenberg, R. S. Greco, Three dimensional staging of breast cancer.
827 *Breast Cancer Res Treat* **41**, 15-19 (1996).
828

829

830

831

832

833 **Figure Legends**

834 **Figure 1. PDA cells adapted to nutrient deprivation exhibit enhanced growth *in vitro* and *in***
835 ***vivo*.** (*A*) Schematic depicting the adaptation process to glucose and glutamine deprivation,
836 followed by selection of adapted "A" clones (C4-C6) derived from SUIT-2 or 8988T human
837 PDA cells that survived and grew in low glucose-low glutamine (L-L) medium, and control non-
838 adapted "NA" clones (C1-C3) derived from parental cells plated at low dilution in high glucose-
839 high glutamine (H-H) medium. (*B*) Relative number of surviving cells from all 7 PDA cell lines
840 that were subjected to L-L medium for a period of 65 days (n = 3). (*C*) Proliferation curves of
841 clonal cells described in *A* that were grown in L-L medium for 7 days (n=5 for SUIT-2 and n=8
842 for 8988T). (*D*) Percent cell death in clones described in *A* (n=5 for SUIT-2 and n=8 for 8988T)
843 that was quantified on Day 4 (SUIT-2) or Day 5 (8988T) of growth in L-L medium. (*E*) Colony
844 formation assay showing number of colonies formed by SUIT-2 or 8988T clones described in *A*
845 that were grown in L-L medium for 7 days (n=6 for SUIT-2 and n=3 for 8988T). (*F*) Three-
846 dimensional (3D) growth assay showing area of spheres formed by SUIT-2 or 8988T cells
847 described in *A* that were grown for 7 days or 10 days, respectively, in L-L medium supplemented
848 with 4% matrigel (n=6 for SUIT-2 and n=8 for 8988T). (*G*) Volumes of orthotopic xenograft
849 PDA tumors quantified by ultrasound that were derived from SUIT-2 clones described in *A* and
850 were injected (750 x 10^3 cells) into the pancreas of 4-6 week old $Rag1^{-/-}$ mice. Tumors were
851 grown for 43 days (n=7 except for NA-C1, n=6); red arrow points at the 2 largest A-C5 tumors at
852 week 4 from mice that died before the week 6 endpoint. (*H*) Weights of orthotopic xenograft
853 SUIT-2 tumors described in *G* that were analyzed at the endpoint, 6 weeks post-tumor cell
854 injection. Data represent the mean ± S.E.M. in *B* and *C*, or mean ± S.D. in *D*-*H*. *$p < 0.05$; **$p <$

855 0.01; ***$p < 0.001$; ****$p < 0.0001$, two-way ANOVA for *B*, *C* and G and one-way ANOVA
856 for *D-F* and *H*, followed by Tukey test.
857
858 **Figure 2. Adapted PDA clones display enhanced *de novo* DNA synthesis and mTORC1**
859 **signaling under nutrient-deprived conditions.** (*A*) Heatmap listing in descending order of
860 statistical significance ($p < 0.05$ by *t* test) metabolites in the purine and pyrimidine synthesis
861 pathways for non-adapted (C1-C3) or adapted (C4-C5) SUIT-2 clones that were treated for 24 h
862 with L-L medium (n=4 replicates per clone). Red indicates higher level and blue lower level,
863 relative to the median for each metabolite across all groups. (*B*) Relative incorporation of
864 radiolabeled U-^{14}C-aspartate into DNA synthesis in non-adapted (NA-C) and adapted (A-C)
865 SUIT-2 clones treated with either L-L or H-H medium for 40 h. Data are presented as relative
866 fold change normalized to NA-C1 under L-L conditions and represent the mean ± S.D. (n=3
867 replicates per clone). *$p < 0.05$; **$p < 0.01$, one-way ANOVA followed by Tukey test. (*C*)
868 Immunoblots of pT389-S6K, pS65-4EBP1, pS1859-CAD and total S6K, 4EBP1, CAD in SUIT-
869 2 or 8988T clones treated with H-H or L-L medium for 24 h. β-actin was used as loading control.
870
871 **Figure 3. Adapted PDA cells induce GS and have enhanced incorporation of nitrogen from**
872 **amino acids into glutamine and nucleotide synthesis.** (*A*) Schematic illustrating glutamate
873 synthesis from α-ketoglutarate (α-KG) and ammonia by glutamate dehydrogenase (GDH) and
874 glutamine synthesis from glutamate and ammonia by glutamine synthetase (GS). In red, are
875 ammonia nitrogens incorporating into glutamate and then glutamine. (*B*) Immunoblots of GS
876 (low and high exposures) and GDH in SUIT-2 or 8988T clones treated with H-H or L-L medium
877 for 24 h. β-actin was used as loading control. (*C*) Fractional labeling of ^{15}N-glutamate and

878 glutamine in SUIT-2 cells treated for 24 h with H-H or L-L medium supplemented with 0.8mM
879 ^{15}N-ammonium chloride. Data are corrected for natural abundance and represent the average of 4
880 replicates per clone per condition ± S.D. (*D*) Schematic illustrating the incorporation of leucine
881 nitrogen (red) into glutamate and then aspartate via transamination reactions catalyzed by
882 branched chain amino acid transaminase BCAT and aspartate transaminase GOT. Glutamate is
883 used to synthesize glutamine via GS and aspartate nitrogen incorporates into newly synthesized
884 nucleotides. (*E*) Heatmap listing in descending order of statistical significance ($p < 0.05$ by *t* test)
885 amino acids in non-adapted or adapted SUIT-2 clones that were treated for 24 h with L-L
886 medium (n=4 per clone per condition). Red indicates higher level and blue lower level, relative
887 to the median for each metabolite across all groups. (*F*) Fractional labeling of metabolites in
888 glutamine and nucleotide synthesis pathways in cells described in *B* grown in media
889 supplemented with 0.4mM ^{15}N-leucine for 24 h. Data represent the average of 4 replicates per
890 clone per condition ± S.D. *$p < 0.05$; **$p < 0.01$; ****$p < 0.0001$, two-way ANOVA for *C*, one-
891 way ANOVA for *F* except for "Glutamine" (two-way ANOVA), followed by Tukey test.
892
893 **Figure 4. PDA adaptation to nutrient deprivation is reversible and associated with changes**
894 **in open chromatin.** (*A*) Schematic depicting the adaptation reversal process where adapted
895 PDA SUIT-2 clones are grown in nutrient replete (H-H) conditions for at least 4 passages, prior
896 to treatment with H-H or L-L medium for 24 h. (*B*) Immunoblots of pT389-S6K (low and high
897 exposures), pS65-4EBP1, pS1859-CAD and total S6K, 4EBP1, CAD and GS (low and high
898 exposures) in SUIT-2 clones (C5, C4 and C6) that were reverse-adapted for over 4 passages and
899 then treated with H-H or L-L medium for 24 h. β-actin or GAPDH was used as loading control.
900 (*C*) Proliferation curves of SUIT-2 clones C5, C4 and C6 from *B* that are either adapted "A" or

901 reverse adapted "RA" for 18 passages, as compared to non-adapted "NA" clones C2, C1 or C3.
902 All clones were grown under L-L conditions for 7 days without media replenishment (n=6). (*D*)
903 Percent cell death in clones described in *C* that were grown under L-L medium for 5 days (n=6).
904 Data represent the mean ± S.E.M. in *C*, and mean ± S.D. in *D*. *$p < 0.05$; **$p < 0.01$; ****$p <$
905 0.0001, two-way ANOVA for *C* and one-way ANOVA for *D*, followed by Tukey test. In *C*, stars
906 indicate statistical significance for A vs NA; A vs RA; RA vs NA on the indicated days. (*E*)
907 Relative mRNA levels of 1,842 genes that were either upregulated or downregulated (>3-fold, q
908 <0.05) in SUIT-2 adapted clones, compared to non-adapted clones; mRNA levels of the
909 corresponding genes in reverse-adapted "RA" clones are shown alongside. Differentially
910 expressed genes were identified by unsupervised k-means clustering. Red, high expression; blue,
911 reduced expression relative to mean expression levels for each gene across all groups (n=3
912 clones per group). (*F*) ATAC-seq data showing significant (>2-fold, q <0.05) changes in
913 chromatin access at enhancers (located >500 bp from transcription start sites) in each of 2
914 independent non-adapted (NA), adapted (A), and reverse-adapted (RA) SUIT-2 clones. (*G*)
915 Correlation of changes in gene expression and nearby (<25 kb) chromatin accessibility for the
916 genes that were induced upon adaptation to nutrient deprivation in SUIT-2 cells. Each dot
917 represents a gene. More gene-linked enhancers (<25 kb) show gains than show losses in
918 accessibility.
919
920 **Figure 5. mTORC1 stabilizes GS protein levels under glutamine deprivation.**
921 (*A*) Immunoblots of GS (low and high exposures), pT389-S6K and total S6K in SUIT-2 adapted
922 clones (C4-C6) that were treated with vehicle control (DMSO) or Torin 1 (40 nM) in L-L
923 medium for 24 h. (*B*) Immunoblots of GS, pS65-4EBP1 and total 4EBP1 in SUIT-2 adapted

924 clonal cells (A-C4) that were treated under L-L medium with control DMSO or Torin 1 (200
925 nM) for a total of 8 h, in the absence or presence of cycloheximide (CHX, 20 μg ml^{-1}) for the
926 indicated times. (*C*) GS protein levels in non-adapted (C1) and adapted (C4) SUIT-2 clones
927 treated in L-L medium with MG-132 (10μM) for the indicated times. (*D*) GS protein levels in
928 SUIT-2 adapted clones treated in L-L medium with either Torin 1 (200 nM) or MG-132 (10μM)
929 alone, or in combination for 12 h (C4) or 8 h (C5, C6). (*E*) Co-immunoprecipitation (IP) blots
930 showing the ubiquitination status of GS in SUIT-2 adapted clones treated in L-L medium, with
931 either Torin 1 (200 nM) or MG-132 (10μM) alone, or in combination for 8 h. Input refers to
932 immunoblots of total GS, pT389-S6K and total S6K levels in whole cell lysates. In *A-E*, β-actin
933 or GAPDH was used as loading control.
934
935 **Figure 6. GS is required for the adaptation-induced growth fitness of PDA cells under**
936 **nutrient deprivation.** (*A*) Proliferation curves of adapted SUIT-2 clonal cells transfected with
937 Doxycycline (Dox)-inducible shScrambled control or shGS hairpins 1 and 2, grown in L-L
938 medium for 7 days in the absence or presence of 1 μg ml^{-1} Dox (n=8). (*B*) Percent cell death in
939 cells described in *A* (n=8) that were grown in L-L medium for 7 days. (*C*) Colony formation
940 assay for cells in *A* that were grown for 10 days, under L-L conditions (n=6). (*D*) Weights of
941 orthotopic xenograft PDA tumors derived from SUIT-2 adapted cells (C4) stably expressing
942 Dox-inducible hairpins described in *A* that were injected (750 x 10^3 cells) into the pancreas of 4-
943 6 week old $Rag1^{-/-}$ mice. Dox was supplemented in the drinking water (2 mg ml^{-1}) 5 days post-
944 injection of cells, and tumors were harvested 33 days later (n=5 shScr -Dox; n=7 shScr + Dox;
945 n=8 shGS#1; n=7 shGS#2). Data represent the mean ± S.E.M. in *A* and mean ± S.D. in *B-D*. *$p <$
946 0.05; **$p < 0.01$; ****$p < 0.0001$, two-way ANOVA followed by Tukey test. (*E*) Immunoblots

947 of GS in cells used for xenografts in *D* showing decreased protein levels, 48 h following

948 treatment with Dox (1 μg ml^{-1}) for inducible knockdown. β-actin was used as loading control.

949 (*F*) Model illustrating a role for GS stabilization in PDA cell adaptation to nutrient deprivation,

950 which leads to enhanced growth fitness. The sketch was created using Biorender.com.

Figure 1

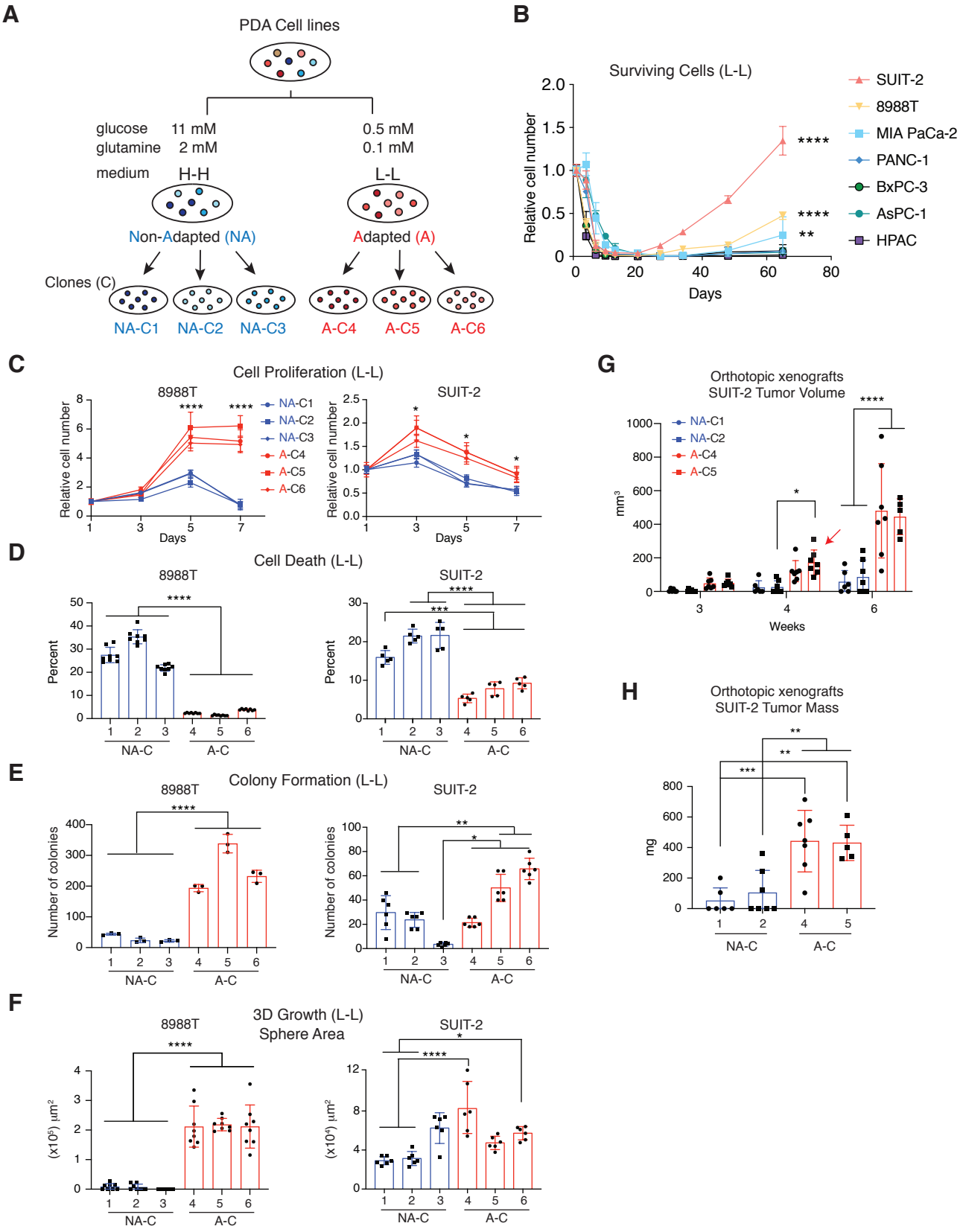
A
PDA Cell lines
glucose 11 mM
glutamine 2 mM
medium H-H
0.5 mM
0.1 mM
L-L
Non-Adapted (NA)
Adapted (A)
Clones (C)
NA-C1
NA-C2
NA-C3
A-C4
A-C5
A-C6
B
Surviving Cells (L-L)
Relative cell number
Days
SUIT-2
8988T
MIA PaCa-2
PANC-1
BxPC-3
AsPC-1
HPAC
C
Cell Proliferation (L-L)
8988T
SUIT-2
Relative cell number
Days
D
Cell Death (L-L)
Percent
NA-C
A-C
E
Colony Formation (L-L)
Number of colonies
F
3D Growth (L-L)
Sphere Area
G
Orthotopic xenografts
SUIT-2 Tumor Volume
mm³
Weeks
H
Orthotopic xenografts
SUIT-2 Tumor Mass
mg

Figure 2

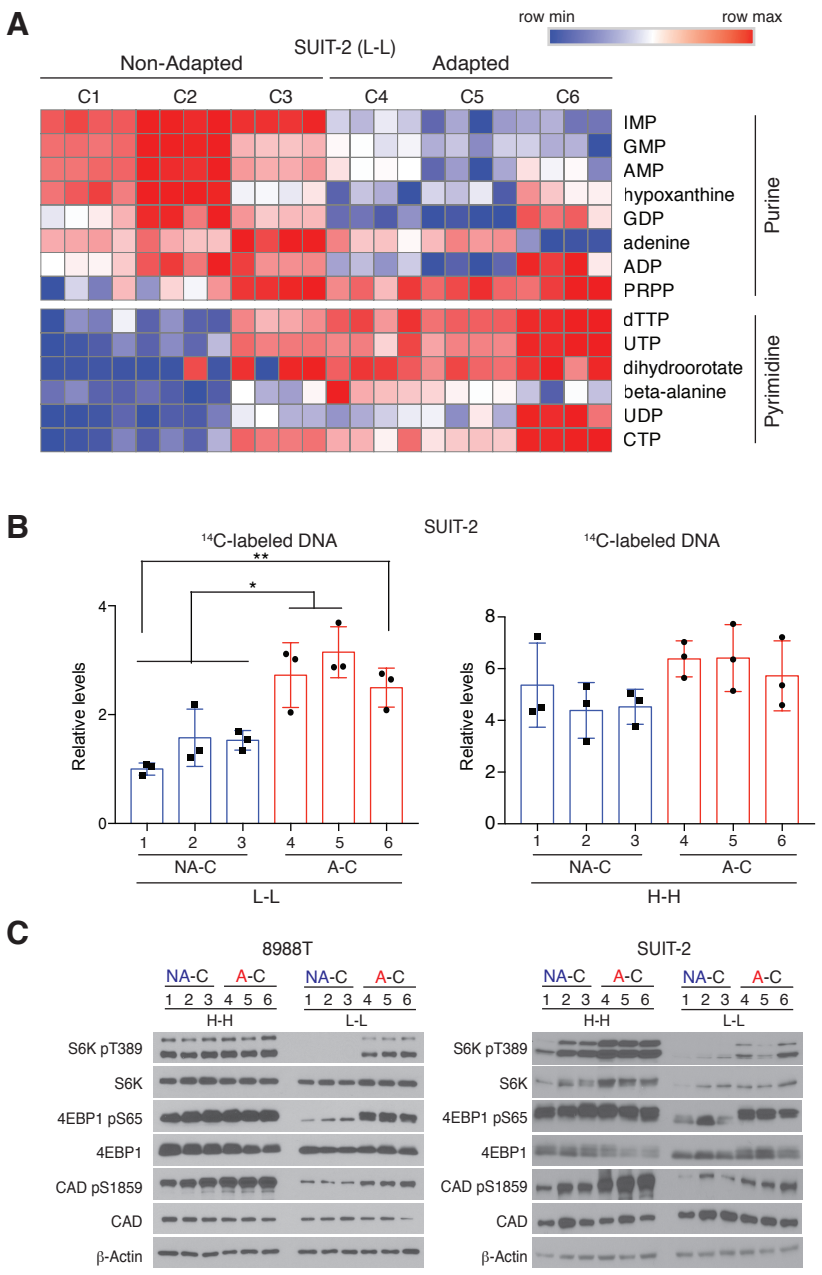
A
row min
row max
SUIT-2 (L-L)
Non-Adapted
Adapted
C1
C2
C3
C4
C5
C6
IMP
GMP
AMP
hypoxanthine
GDP
adenine
ADP
PRPP
Purine
dTTP
UTP
dihydroorotate
beta-alanine
UDP
CTP
Pyrimidine
B
SUIT-2
14C-labeled DNA
14C-labeled DNA
Relative levels
NA-C
A-C
L-L
H-H
C
8988T
SUIT-2
NA-C
A-C
H-H
L-L
S6K pT389
S6K
4EBP1 pS65
4EBP1
CAD pS1859
CAD
β-Actin

Figure 3

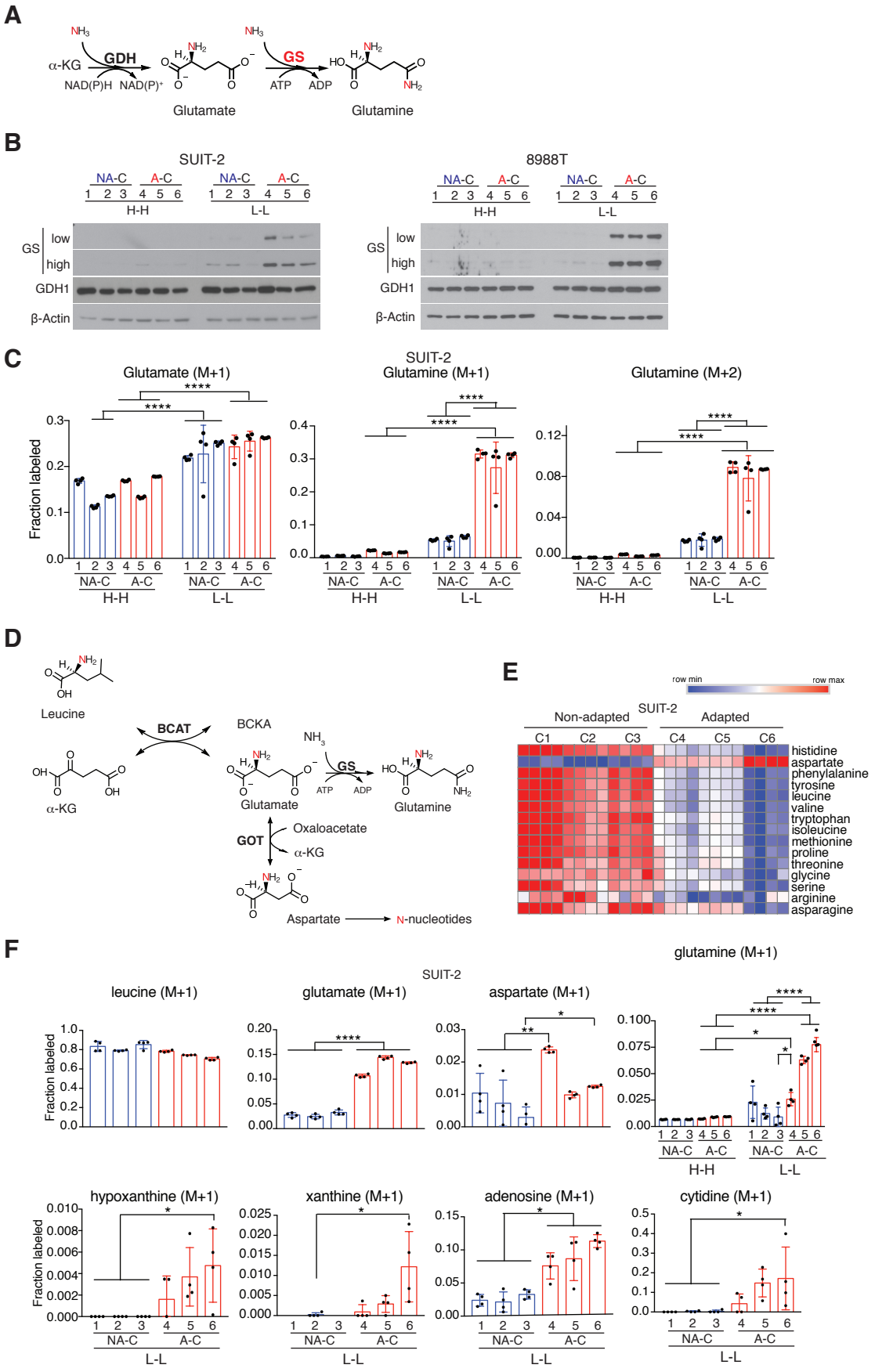
A
NH3
GDH
α-KG
NAD(P)H NAD(P)+
Glutamate
NH3
GS
ATP ADP
Glutamine
B
SUIT-2
8988T
NA-C A-C NA-C A-C
1 2 3 4 5 6 1 2 3 4 5 6
H-H L-L
GS low high
GDH1
β-Actin
C
Glutamate (M+1)
SUIT-2
Glutamine (M+1)
Glutamine (M+2)
Fraction labeled
****
NA-C A-C
H-H L-L
D
Leucine
BCAT
α-KG
BCKA
GS
ATP ADP
Glutamate
Glutamine
GOT
Oxaloacetate
α-KG
Aspartate
N-nucleotides
E
row min
row max
SUIT-2
Non-adapted
Adapted
C1 C2 C3 C4 C5 C6
histidine
aspartate
phenylalanine
tyrosine
leucine
valine
tryptophan
isoleucine
methionine
proline
threonine
glycine
serine
arginine
asparagine
F
SUIT-2
leucine (M+1)
glutamate (M+1)
aspartate (M+1)
glutamine (M+1)
Fraction labeled
NA-C A-C
H-H L-L
hypoxanthine (M+1)
xanthine (M+1)
adenosine (M+1)
cytidine (M+1)
L-L

Figure 4

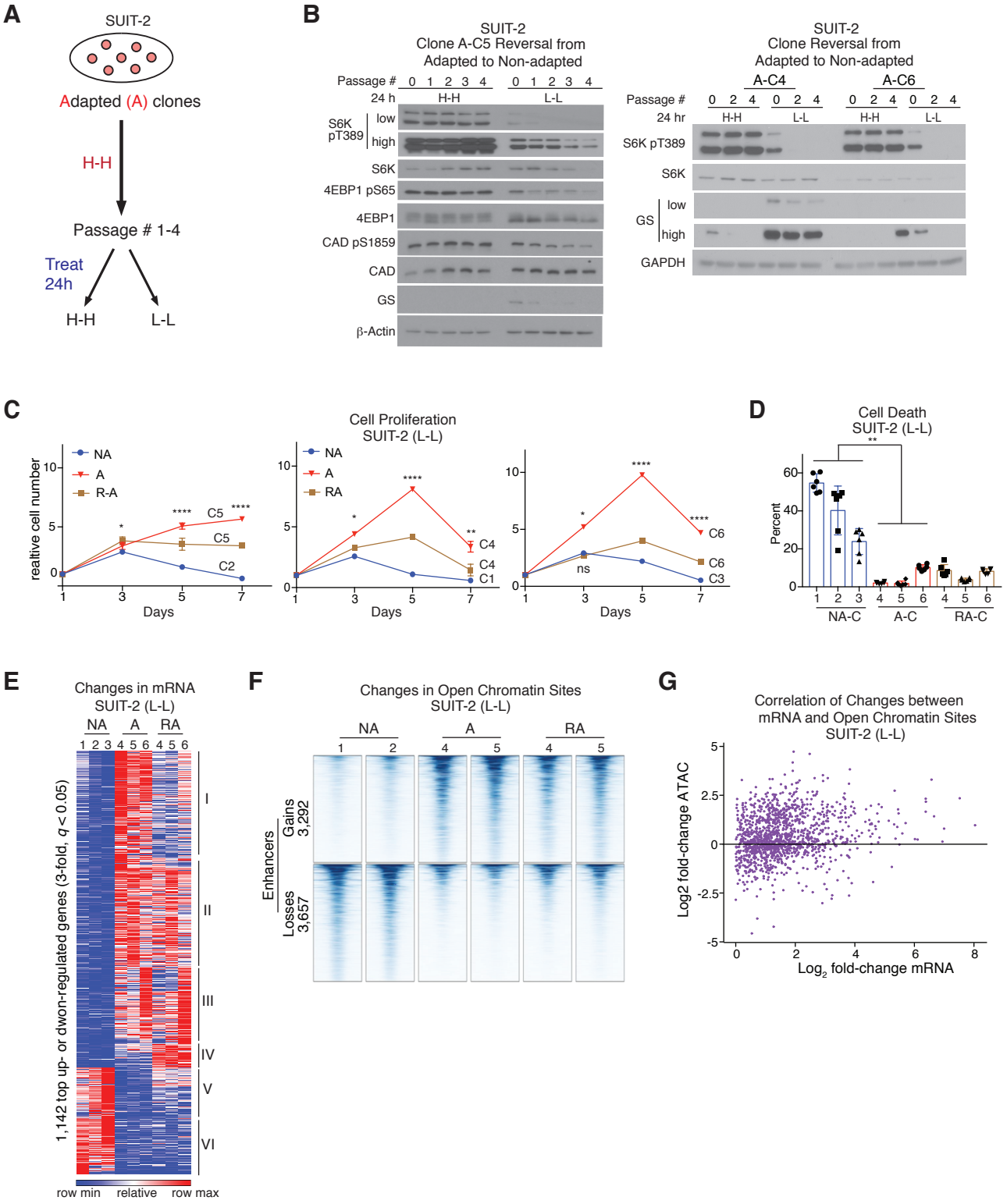
A
SUIT-2
Adapted (A) clones
H-H
Passage # 1-4
Treat 24h
H-H
L-L
B
SUIT-2
Clone A-C5 Reversal from Adapted to Non-adapted
Passage #
24 h
H-H
L-L
S6K pT389
low
high
S6K
4EBP1 pS65
4EBP1
CAD pS1859
CAD
GS
β-Actin
SUIT-2
Clone Reversal from Adapted to Non-adapted
A-C4
A-C6
24 hr
GAPDH
C
Cell Proliferation
SUIT-2 (L-L)
NA
A
R-A
RA
realtive cell number
Days
C5
C2
C4
C1
C6
C3
ns
D
Cell Death
SUIT-2 (L-L)
Percent
NA-C
A-C
RA-C
E
Changes in mRNA
SUIT-2 (L-L)
NA
A
RA
1,142 top up- or dwon-regulated genes (3-fold, q < 0.05)
row min
relative
row max
F
Changes in Open Chromatin Sites
SUIT-2 (L-L)
Enhancers
Gains 3,292
Losses 3,657
G
Correlation of Changes between mRNA and Open Chromatin Sites
SUIT-2 (L-L)
Log2 fold-change ATAC
Log2 fold-change mRNA

Figure 5

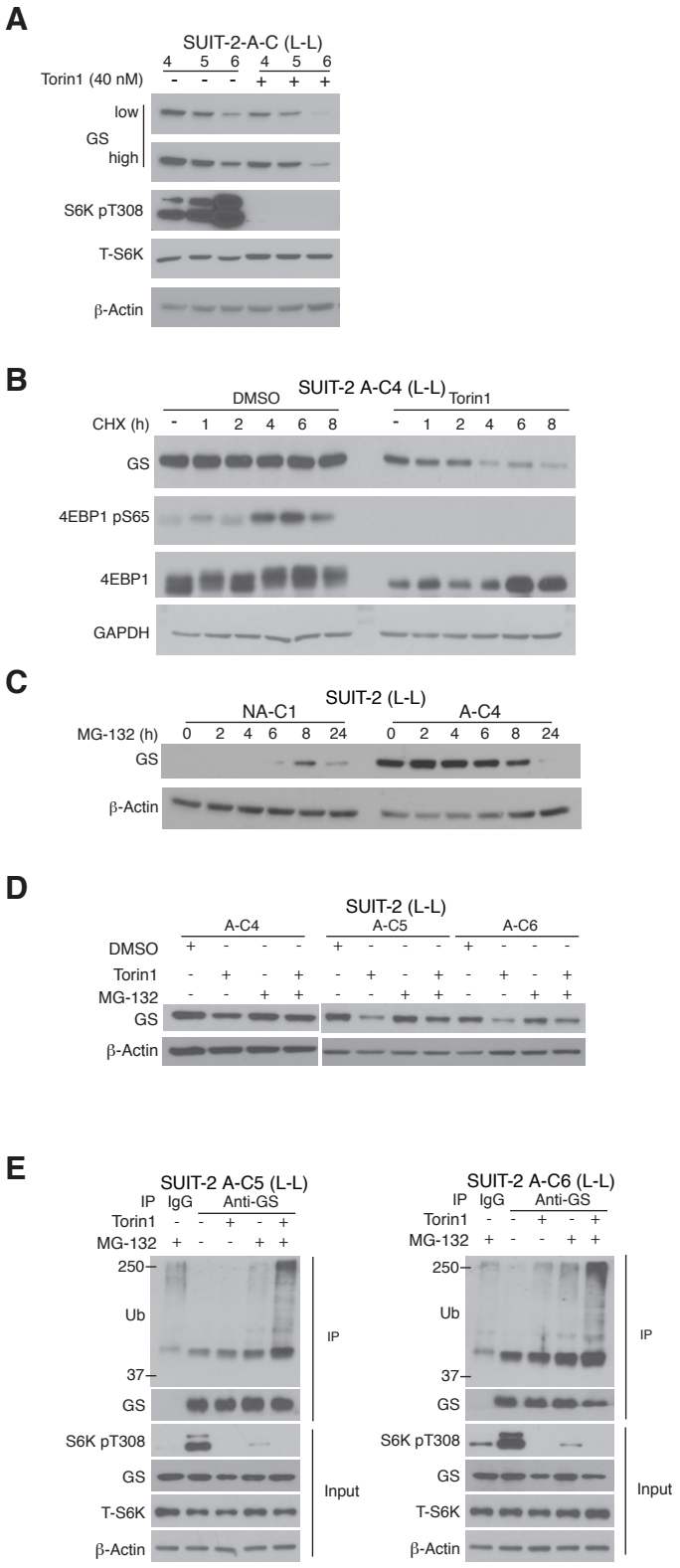
A
SUIT-2-A-C (L-L)
4 5 6 4 5 6
Torin1 (40 nM) - - - + + +
GS
low
high
S6K pT308
T-S6K
β-Actin
B
SUIT-2 A-C4 (L-L)
DMSO
Torin1
CHX (h) - 1 2 4 6 8 - 1 2 4 6 8
GS
4EBP1 pS65
4EBP1
GAPDH
C
SUIT-2 (L-L)
NA-C1
A-C4
MG-132 (h) 0 2 4 6 8 24 0 2 4 6 8 24
GS
β-Actin
D
SUIT-2 (L-L)
A-C4
A-C5
A-C6
DMSO
Torin1
MG-132
GS
β-Actin
E
SUIT-2 A-C5 (L-L)
SUIT-2 A-C6 (L-L)
IP IgG Anti-GS
Torin1
MG-132
250
Ub
37
GS
IP
S6K pT308
GS
T-S6K
β-Actin
Input

Figure 6

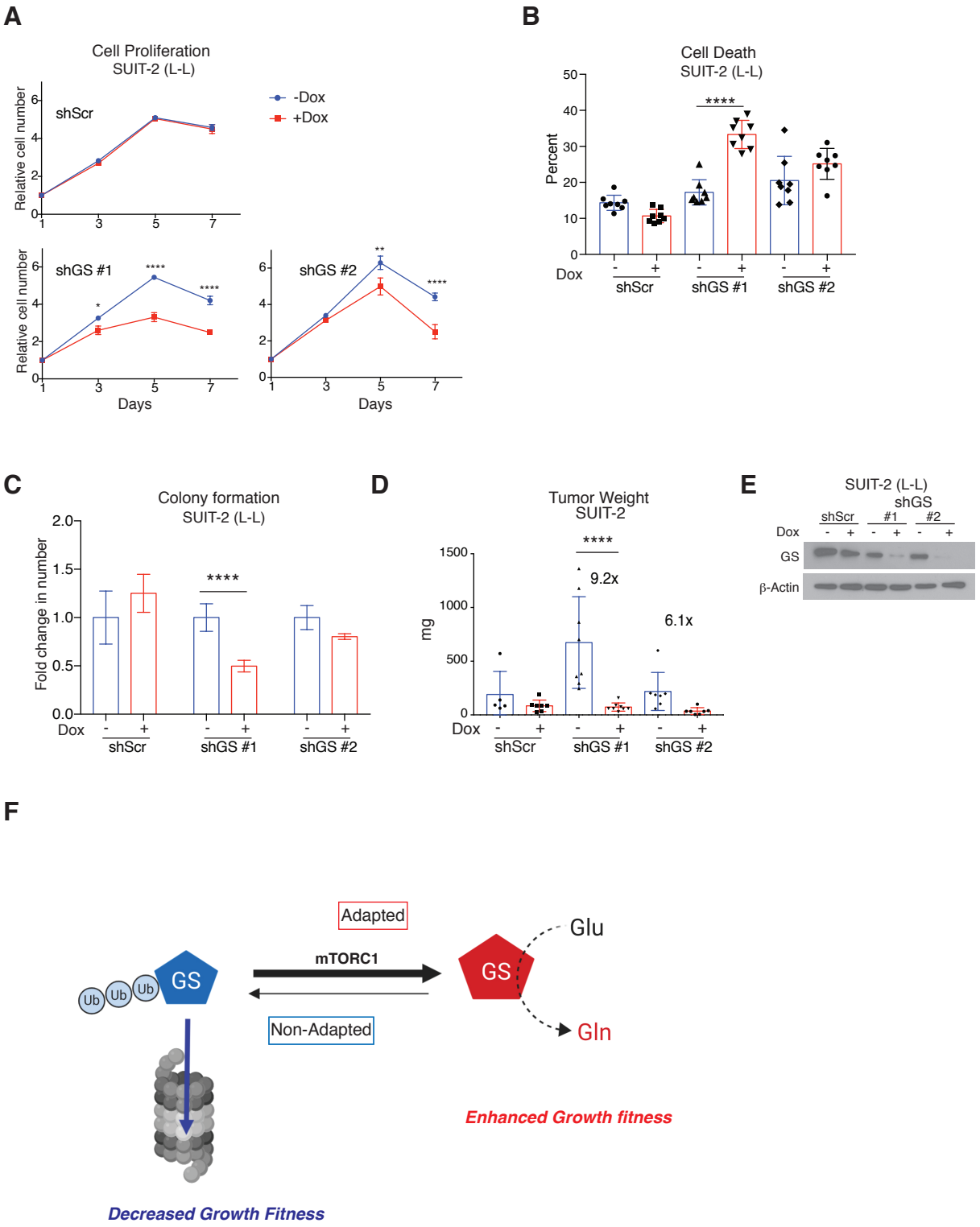
A
Cell Proliferation
SUIT-2 (L-L)
-Dox
+Dox
shScr
shGS #1
shGS #2
Relative cell number
Days
B
Cell Death
SUIT-2 (L-L)
Percent
Dox
shScr
shGS #1
shGS #2
C
Colony formation
SUIT-2 (L-L)
Fold change in number
D
Tumor Weight
SUIT-2
mg
9.2x
6.1x
E
SUIT-2 (L-L)
shGS
GS
β-Actin
F
Adapted
mTORC1
Non-Adapted
Ub
GS
Glu
Gln
Enhanced Growth fitness
Decreased Growth Fitness